ICES
CIEM

International Council for
the Exploration of the Sea

Conseil International pour
l'Exploration de la Mer

Modelled marine migrations of Atlantic salmon post-smolts from Irish and Scottish rivers vary interannually with local currents and salinity

Aislinn Borland [1,*], Neil Banas [1], Alejandro Gallego[2], Douglas Speirs[1], Emma Tyldesley [1], Colin Bull [3,4]

[1]Department of Mathematics and Statistics, University of Strathclyde, 26 Richmond Street, Glasgow G1 1XH, United Kingdom
[2]Marine Laboratory Aberdeen, Marine Directorate, 375 Victoria Road, Aberdeen AB11 9DB, United Kingdom
[3]Atlantic Salmon Trust, Bridge of Earn, Perthshire PH2 9HN, United Kingdom
[4]Institute of Aquaculture, University of Stirling, Stirling FK9 4LA, United Kingdom

*Corresponding author: Aislinn Borland, Department of Mathematics and Statistics, University of Strathclyde, 26 Richmond Street, Glasgow G1 1XH, United Kingdom. E-mail: aislinn.borland@strath.ac.uk

Abstract

Atlantic salmon (*Salmo salar*) populations have suffered declines across their range in recent decades, largely attributed to decreasing marine survival rates. The first few months at sea are thought to be a time of particular vulnerability, but investigation into drivers of survival is limited by a lack of knowledge of migratory paths. Here, we model the early marine migration of Atlantic salmon from Scottish and Irish rivers over 27 years. Movement is simulated over the first 3 months at sea using a Lagrangian particle tracking model (FVCOM i-state configuration model) coupled with an active swimming model that is dependent on ocean currents, salinity, and compass direction. Our model is driven by the reanalysis of a high-resolution ocean model (Scottish Shelf Waters Reanalysis Service). Differences in the speed of migrations, the proportion of time spent in different oceanographic regions, and the proportion of migrations reaching the Norwegian Sea are seen between years. These differences are related to changes in local ocean conditions: years with lower on-shelf salinity, stronger on-shelf northwest currents, and stronger shelf-edge currents were associated with greater migration success. Within years, differences in modelled migrations between rivers were best explained by their minimum distance from the continental shelf edge.

Keywords: Atlantic salmon; *Salmo salar*; marine migration; oceanography; Northeast Atlantic; individual-based model; particle tracking; environmental variability

Introduction

Atlantic salmon (*Salmo salar*) populations once thrived around Europe and North America, but in recent decades there have been declines in their numbers across the North Atlantic (ICES 2024), likely caused by decreasing marine growth and survival rates (Friedland et al. 2009, Pardo et al. 2021). However, the mechanisms behind these shifts remain uncertain, and a more comprehensive understanding of the marine migration routes is required to investigate these mechanisms (ICES 2020, 2023) and to help develop more effective future management strategies (Bull et al. 2022). In particular, a better understanding of year-to-year changes in migrations is key to understanding year-to-year changes in marine survival rates, as the spatial and temporal variability in physical ocean conditions and in prey fields (Bartsch and Coombs 1997, van Deurs et al. 2013) mean that variability in migration pathways will likely influence the physical conditions and feeding opportunities encountered by salmon, factors that have been shown to influence survival (Friedland et al. 1998, 2012, Furey et al. 2015, Tyldesley et al. 2024).

Atlantic salmon from Southern European populations (including Scotland and Ireland) enter the sea in April and May at around 10–20 cm in body length and spend up to 4 years at sea before returning to their natal rivers as adults to spawn (Aas et al. 2010). Until the end of their first winter at sea,

they are known as post-smolts (Allan and Ritter 1977). Post-smolts initially migrate towards feeding grounds in the Norwegian Sea (Gilbey et al. 2021, Fig. 1) and several targeted sampling studies have found relatively high concentrations of post-smolts at the European continental shelf edge (Shelton et al. 1997, Holm et al. 2000, Utne et al. 2020, Gilbey et al. 2021). Telemetry (tagging) studies provide valuable information on the early migratory movements of salmon (e.g. Økland et al. 2006, Thorstad et al. 2013, Barry et al. 2020, Newton et al. 2021, Lilly et al. 2022,2023, Rodger et al. 2024) or on the later movements of returning adult salmon (e.g. Kennedy et al. 2023), but due to limitations on the various telemetric methods, this approach has not yet revealed a full marine migration pathway in Atlantic salmon post-smolts.

Modelling approaches that integrate environmental, physiological, and behavioural elements to simulate migrations offer an opportunity to address knowledge gaps. Particle tracking models coupled with active swimming models have been used for this purpose in several cases (Booker et al. 2008, Mork et al. 2012, Byron et al. 2014, Moriarty et al. 2016, Ounsley et al. 2020, Newton et al. 2021). Varied swimming models were applied across these studies since migration behaviour is expected to vary regionally and with environmental conditions (Byron and Burke 2014). With the exception of the 24-year modelling study by Moriarty et al. (2016) in the
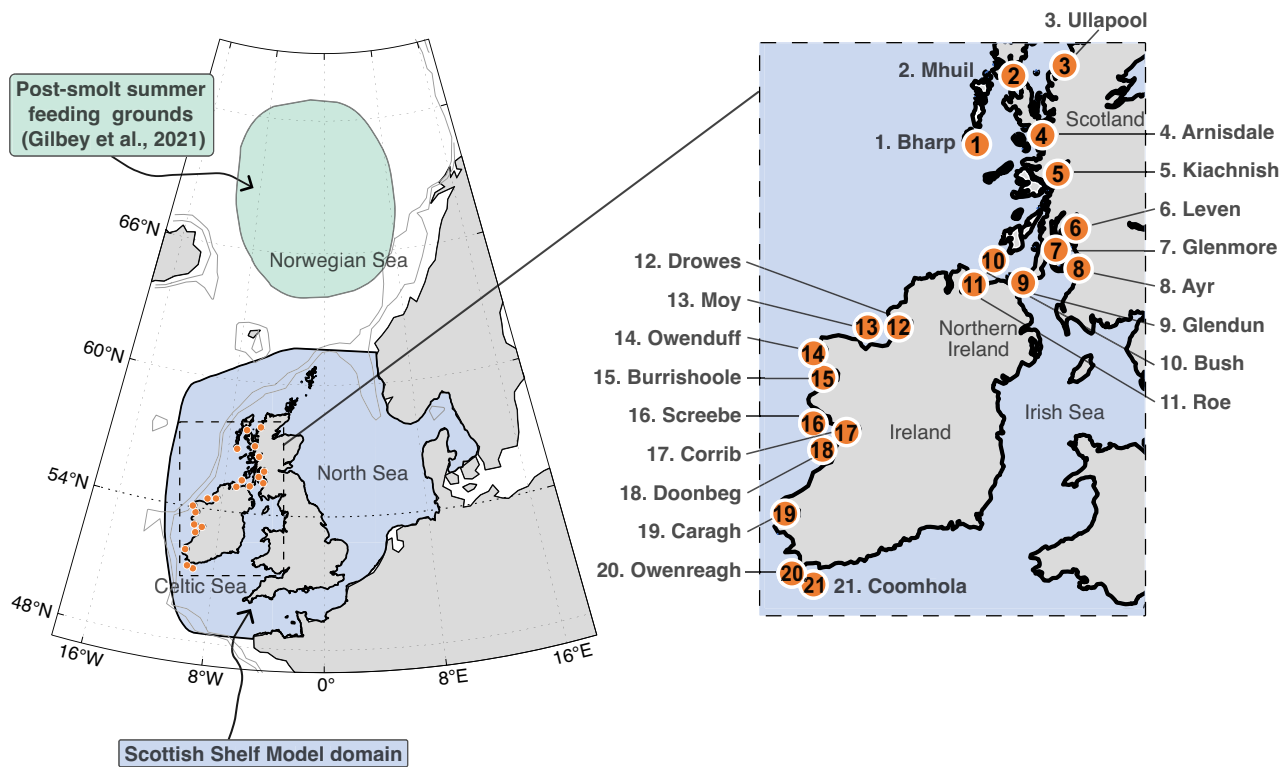
Figure 1. Summer feeding grounds of Atlantic salmon post-smolts (*Salmo salar*), the Scottish Shelf Model domain, and the rivers where migrations are modelled. Isobaths at 200 m and 400 m indicate the location of the continental shelf edge.

Northwest Atlantic, previous particle tracking studies have focused on simulating migrations in just one or two years (Booker et al. 2008, Mork et al. 2012, Ounsley et al. 2020, Newton et al. 2021). Interannual variation has therefore not been well-considered over extended periods of time in models of post-smolt migration from European rivers.

Here, we simulate the initial post-smolt migration towards the Norwegian Sea from a group of Scottish, Northern Irish, and Irish rivers (Fig. 1) over a 27-year period. Large-scale ocean and atmospheric processes influence physical conditions across this region. Expansion or contraction of the subpolar gyre (SPG) causes changes to large-scale advective pathways in the northeast Atlantic, influencing water salinity, temperature, and productivity (Hátún et al. 2009, Koul et al. 2020). Changes in the North Atlantic Oscillation (NAO), measured by the sea-level pressure difference between a region of high pressure (the Subtropical High, in the Azores) and a region of low pressure (the Subpolar Low, in Iceland) relate to changes in westerly winds, which can impact circulation and water mass properties in the North Atlantic region (Hurrell 1995, Sarafanov 2009). The NAO index has also been correlated with salmon growth and survival (Jonsson and Jonsson 2004, Peyronnet et al. 2008).

Most of the region in Fig. 1 lies on the European continental shelf. In addition to basin-scale ocean and atmospheric processes, shelf seas are influenced locally by surface warming and heat loss, freshwater input, tides, and wind forcing (Simpson and Sharples 2012). These processes cause small-scale spatial and temporal variability in water properties and circulation on the northwest European continental shelf (Holt et al. 2012, Jones et al. 2018). At the shelf edge, the sudden change in bathymetry induces a current flowing parallel to

the isobaths (Simpson and Sharples 2012), i.e. parallel to the shelf edge. The European shelf-edge current exhibits seasonal and interannual variability (Xu et al. 2015), with much of the interannual variability explained by the North Atlantic Current (NAC; Houpert et al. 2020). The NAC is itself related to the SPG: a faster and more eastward expanded NAC current pathway is seen in periods of a stronger SPG, causing a strengthened shelf-edge current (Marsh et al. 2017, Holliday et al. 2020, Clark et al. 2022). A long-term decrease in the strength of the shelf-edge current has also been identified (Xu et al. 2015, Clark et al. 2022). Given there have been several recaptures of post-smolts at the continental shelf edge, we hypothesize that this current is an important feature used by post-smolts during their migration towards the Norwegian Sea. Variability in this current might therefore influence migrations.

Simulating post-smolt migrations requires an understanding of the potential navigational cues employed. Migratory animals are known to use multiple navigational cues at once, or in sequence, along their journey, with 'signposts' in the form of magnetic cues or physical properties dictating the switch between behaviours (Kashetsky et al. 2021). Gradients of environmental variables can be used to aid migration and even extrapolated beyond the area experienced by an individual (Kashetsky et al. 2021). Intraspecific variation in how navigational behaviours are employed is found between and even within populations (Chapman et al. 2014).

Several mechanisms have been suggested as potential navigational cues for Atlantic salmon. First, salmon may use the vertical current shear between water layers to detect small changes in flow, a mechanism that could allow them to follow ocean currents (Døving and Stabell 2003). Local currents have

been identified as a navigational cue during estuarine migration, with post-smolts actively migrating primarily during ebb tides (Lacroix and McCurdy 1996, Lacroix et al. 2004, Main 2021, Lilly et al. 2022). On a larger scale, it has been suggested that post-smolts might use the North Atlantic subpolar gyre current to migrate (Dadswell et al. 2010). A second potential navigation cue is salinity, which has been identified as a likely 'signpost' in eel migration (Schabetsberger et al. 2016, Cresci 2020). Salmon have a highly sensitive olfactory system, which could allow them to detect small chemical differences between water masses (Døving and Stabell 2003), allowing them to follow salinity cues. Increased swimming speed has been seen in post-smolts experiencing a positive salinity gradient in coastal and estuarine waters (Hedger et al. 2008, Martin et al. 2009). Preferences for certain salinity ranges could relate to the choice of certain water masses, possibly for their associated prey fields, or perhaps for the currents signified by the water mass (e.g. the continental shelf-edge current). Third, several studies have shown the response of both Pacific and Atlantic salmon to magnetic cues (Quinn 1980, Taylor 1986, Putman et al. 2014, Minkoff et al. 2020), and Moore et al. (1990) found magnetite crystals in the lateral line of Atlantic salmon smolts and adults, suggesting a mechanism by which salmon can utilize magnetic cues in migration.

Migration modelling also requires estimates of marine swimming speeds. Post-smolt marine swimming speeds can be inferred from recaptures (10–26 km/day, Thorstad et al. 2012) or estimated from acoustic telemetry, with speeds measured in Scotland and Ireland ranging from 9.7 to 53.8 km/day, with variation in speeds seen both between and within river populations (Main 2021, Lilly et al. 2022, 2023, Rodger et al. 2024). Estimates of swimming speed are calculated using the straight-line distance between detections, but post-smolts are likely to take a more convoluted route, meaning measured speeds are the minimum possible speeds. Differences in the swimming speeds measured through telemetry work also reflect the influence of local water currents, or potentially other changing conditions such as salinity, and differences in migration strategy, for example, foraging vs. moving as quickly as possible to the goal location.

The aims of this study are: (1) to develop a post-smolt migration model applicable to the initial period of marine movement within the Scottish Shelf Model domain for the rivers displayed in Fig. 1; (2) to examine interannual variation in migratory paths and metrics of migrations; and (3) to investigate the possible mechanisms behind this variation.

Methods

In this study, we used a Lagrangian particle tracking model (FVCOM i-state Configuration Model) driven by a high-resolution ocean model hindcast (Scottish Shelf Waters Reanalysis Service), which provided 27 years of data (1993–2019) over the Scottish Shelf Model domain (Fig. 1). This was combined with an active swimming model that was developed to simulate the movement of salmon from Scottish, Irish, and Northern Irish rivers over the first three months at sea. Modelled migrations were compared with observed locations of migrating post-smolts, and we considered whether variability in modelled migrations was related to variability in environmental conditions or to geographical differences between rivers. Finally, interannual variability in modelled migrations was compared with Atlantic salmon marine survival

rates from rivers within our region of focus. All model assumptions are detailed in the text and are additionally summarized in the Supplementary Information.

Migration simulations were run on the ARCHIE-WeSt High Performance Computer (www.archie-west.ac.uk) and the analysis of results was conducted in MATLAB (Mathworks Inc. 2021).

Lagrangian particle tracking

The offline particle tracking software FISCM (FVCOM i-state configuration model; Liu et al. 2015, Ounsley et al. 2020, https://github.com/GeoffCowles/fiscm/tree/ounsley_et_al_2019) was used to simulate the movement of Atlantic salmon post-smolts, where each particle represented a post-smolt. The velocities of individual particles were calculated at each timestep and then integrated using the 4th-order Runge–Kutta method to update particle positions. For a particle $\mathbf{x_t} = (x_t, y_t)^T$ at longitude x_t and latitude y_t at time t, position at the next timestep $(t + \delta t)$ is given by:

$$x_{t+\delta t} = \mathbf{x_t} + \left((\mathbf{u_t} + \mathbf{g_t})\, \delta t + Q\sqrt{2K\delta t} \right) \mathbf{c} \qquad (1)$$

where $\mathbf{u_t} = (u, v)^T$ is the current velocity at time t in ms^{-1}, $\mathbf{g_t} = (g_x, g_y)^T$ is the active swimming velocity of particles at time t in ms^{-1}, Q is normally distributed with mean 0 and standard deviation 1, K is the horizontal diffusion coefficient, taken to be $10\ m^2 s^{-1}$, and $\mathbf{c}$ represents the conversion from metres to degrees longitude/latitude, taken here as $\mathbf{c} = (8.99322 \times 10^{-6} \cos(y_{t+\delta t}),\ 8.99322 \times 10^{-6})^T$. The timestep δt is discussed in section 'Model timestep'.

Scottish Shelf Model and the Scottish Shelf Waters Reanalysis Service

Currents $\mathbf{u_t}$ were derived from the Scottish Shelf Waters Reanalysis Service 3.02 (SSW-RS) reanalysis of the Scottish Shelf Model (SSM). The SSM is a hydrodynamic model covering the seas around the British Isles (Murray 2017). It is an implementation of the Finite Volume Community Ocean Model (FVCOM; Chen et al. 2003), meaning the grid is irregular and unstructured, made up of triangles which vary in shape and size. This type of model allows the resolution of the grid to vary so that coastal features can be resolved on a fine scale. Horizontal grid resolution ranges from 1 km around the coast to 20 km off the shelf. The model uses a hybrid terrain-following coordinate system, with 20 depth layers. The depth levels are evenly distributed in water of depth <120 m. In water ≥120 m, there are five fixed depth levels at the top of the water column, which are 3, 6, 7, 7, and 7 m thick and lie at depths of 1.5, 6, 12.5, 19.5, and 26.5 m, respectively, and two fixed depth levels at the bottom of the water column, both of which are 6 m thick and lie 3 and 9 m above the seabed (Barton et al. 2022). The remaining 13 depth levels are evenly distributed across the remainder of the water column.

The SSSW-RS is a 27-year (1993–2019) physical reanalysis of the Scottish Shelf Model (Barton et al. 2022). Along the open Atlantic boundary, the model was forced by the Atlantic-European North West Shelf-Ocean Physics Reanalysis (https://doi.org/10.48670/moi-00059). At the open Baltic boundary, the model was forced by the Baltic Sea Physics Reanalysis (https://doi.org/10.48670/moi-00013). Atmospheric forcing, including wind velocity, was provided by the Copernicus ERA5 global reanalysis (Hersbach et al. 2020).

Riverine inputs comprised of volume fluxes from both the Hydrological Predictions for the Environment over Europe dataset (Arheimer et al. 2020) and the Centre for Ecology and Hydrology (CEH) Grid-to-Grid (G2G) model (Bell et al. 2009). Daily sea surface temperature (SST) from the ODYSSEA satellite dataset (Autret et al. 2020) was assimilated into the model. Bathymetry was taken from the AMM15 model from the European Marine Observation and Data Network (Martín Míguez et al. 2019). Model temperature and salinity from the SSW-RS have been compared to in situ temperature and salinity profiles, with good agreement in the spatial and temporal patterns (Barton et al. 2024).

The SSW-RS is available as hourly and daily (24-hour average) data outputs. The choice between these two formats is discussed with the choice of timestep in section 'Model timestep'. Currents from the SSW-RS were interpolated at each timestep to present particle position, providing $\mathbf{u_t}$ in Equation (1).

Active swimming model

We propose an active swimming model composed of three behaviours: swimming in the direction of local currents, swimming in the direction of the local salinity gradient, and directional swimming on a constant compass bearing (magnetic cue). Together, these provided $\mathbf{g} = (g_x, \, g_y)^T$ in Equation (1), with

$$\mathbf{g} = w_c \, \mathbf{g_c} + w_s \, \mathbf{g_s} + w_d \, \mathbf{g_d} \qquad (2)$$

where $\mathbf{g_c}, \mathbf{g_s}$ and $\mathbf{g_d}$ are the current, salinity, and directional active swimming component vectors, and w_c, w_s and w_d are the respective scalar weights, where $w_c, w_s, w_d \geq 0$.

The current-following behavioural component $\mathbf{g_c}$ was given by

$$\mathbf{g_c} = s \, L \, \left(\frac{\mathbf{u}}{|\mathbf{u}|} \right) \qquad (3)$$

where s is the swimming speed in body lengths per second, L is the body length of the fish in metres (see section 'Growth model' below), and $\mathbf{u} = (u, \, v)^T$ is the current velocity.

The salinity-gradient-following component was then given by

$$\mathbf{g_s} = s \, L \, \frac{\nabla S}{|\nabla S|_{median} + |\nabla S|} \qquad (4)$$

where ∇S is the salinity gradient, calculated as detailed in section 'Salinity gradient calculation'. The above format represents a saturation function where $|\nabla S|_{median}$ (the median salinity gradient magnitude) is the half-saturation point. To determine $|\nabla S|_{median}$, the salinity gradient was calculated across the whole SSW-RS domain in April-May over 5 years, giving a value of $|\nabla S|_{median} = 0.0045$ psu/km.

The directional component $\mathbf{g_d}$ was defined as

$$\mathbf{g_d} = s \, L \, R \, \frac{|\theta - \theta_{bias}|}{\pi} \, \mathbf{q} \qquad (5)$$

where θ is the current direction of movement (in radians; measured anticlockwise from the positive direction of the x-axis), θ_{bias} is the preferred direction of movement, $\mathbf{q} = \begin{pmatrix} \cos \theta_{bias} \\ \sin \theta_{bias} \end{pmatrix}$ and

$$R = \begin{cases} 0 & \text{before first instance of water} > 200 \text{ m deep} \\ 1 & \text{after first instance of water } > 200 \text{ m deep.} \end{cases}$$

The preferred direction of movement θ_{bias} was chosen to be $\pi/5$ (equivalent to a bearing of 54° from north) as this is approximately the angle of the continental shelf edge in our domain. The inclusion of R means that modelled post-smolts initially used only currents and salinity to navigate, but upon reaching deeper waters (approximately at the continental shelf edge), they additionally used the directional cue. Depth therefore acted as a 'signpost' in our model, signalling the switch from one migratory behaviour to another (Kashetsky et al. 2021). We do not propose that post-smolts can directly detect the bottom bathymetry; rather they might use chemical or optical cues associated with the transition from shelf to open-ocean water.

While the maximum magnitude of each of the three components $\mathbf{g_c}, \mathbf{g_s}$ and $\mathbf{g_d}$ are all $s \, L$, their magnitudes are not necessarily equal at any given time. This reflects the use of different navigational cues throughout the migration, depending on the relative strength of each. For example, the $\mathbf{g_s}$ term will be small when there is a weak salinity gradient, meaning salinity will not be the primary method of navigation. Similarly, $\mathbf{g_d}$ is at a minimum (zero) when movement is already in the preferred direction and reaches a maximum when movement is in the opposite direction. Consequently, the swim speed s acts as an upper bound, but modelled post-smolts will almost always be moving slower than this. We enforced that $\sqrt{w_c^2 + w_s^2 + w_d^2} = 1$ in the parameter testing process (discussed in section 'Parameter optimization and sensitivity') to ensure that duplicate combinations of the weights and s were not tested.

Salinity gradient calculation

The gradient of a scalar field is the direction and magnitude of the greatest rate of increase of the field values. We calculated the surface salinity gradient ∇S at each point p using all cells within a radius ϵ of p. This ensured that the gradient was calculated on a constant scale across the domain despite the irregular grid. This method is also applicable to points lying near or on the coastline. The salinity gradient was calculated using the uppermost layer of the SSW-RS, which is the top 5% of the water column in water <120 m deep, or a fixed depth layer of 0–3 m in water greater than 120 m deep. This meant that salinity was calculated over a similar, but not identical, surface layer across the SSM domain.

The grid cells surrounding p within the radius ϵ were divided into quadrants (q_1, q_2, q_3, q_4), as in Fig. 2. The mean value of S was calculated in each quarter $i = (1, \, 2, \, 3, \, 4)$ and denoted as S_{q_i}. Similarly, the mean distance (in kilometres) from the cells in each quarter i to p was calculated and denoted d_i. If any quarter does not contain any grid cells (e.g. if it covers land), then $S_{q_i} = 0$ and $d_i = 0$. The salinity gradient ∇S at a point p was then given by

$$\nabla S(p) = \left(\frac{S_{q_1} - S_{q_3}}{d_1 + d_3}, \, \frac{S_{q_2} - S_{q_4}}{d_2 + d_4} \right) \qquad (6)$$

with units psu/km.

The parameter ϵ represents the area in which post-smolts can detect or extrapolate conditions, allowing them to decide which direction to swim. A smaller value of ϵ hence represents the use of small-scale patterns in salinity for navigation, while a larger value simulates the use of large-scale spatial patterns. Figure 3(a)–(c) shows the salinity gradient magnitude calculated with $\epsilon = 5$ km, $\epsilon = 10$ km, and $\epsilon = 50$ km.
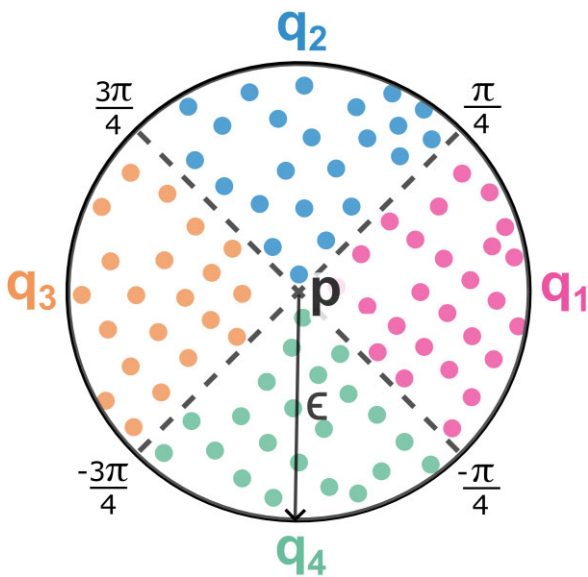
Figure 2. Schematic of salinity gradient calculation. Quadrants q_1, q_2, q_3, q_4 are shown, with dots representing points in the salinity field on the irregular Scottish Shelf Model (SSM) grid.

Increasing the radius of calculation smoothed the spatial patterns in salinity. With this method, the salinity gradient was not calculated at points within the domain where the grid resolution is greater than ϵ. This is seen through the white patches in the $\epsilon = 5$ km and $\epsilon = 10$ km cases. Figure 3(d)–(f) shows the salinity gradient with the saturation function of Equation (4) for $\mathbf{g_s}$ applied. This function rescaled the gradient to a more normal distribution and ensured all values lie between 0 and 1.

Unfortunately, sufficient information is not currently available to constrain ϵ on the basis of physical measurements or knowledge of post-smolt migration behaviour. However, when calculating gradients of mesozooplankton concentration in a model simulating blue whiting migration, Dolmaire (2022) suggested that this value should be no greater than the distance travelled in one timestep so that individuals could detect conditions within a radius that they were able to cover. The final choice of ϵ is hence discussed in section 'Model timestep' alongside the choice of timestep δt.

Model timestep

The choice of timestep δt took into account several factors:

(1) The desired timescale of navigational choices. This relates to the radius of salinity gradient detection ϵ (i.e. the area in which simulated post-smolts can detect conditions before deciding which direction to swim).
(2) The time resolution of modelled ocean conditions used to make navigational choices (i.e. the time resolution of the SSW-RS).
(3) Computational accuracy and efficiency.

Regarding the time resolution (2), two options were available to force the model: the hourly or daily SSW-RS files. The former would be suitable for simulating fine-scale movement in relation to tidal currents with a small timestep, while the daily files would be suitable for simulating larger-scale navi-

gational choices with a larger timestep, based on residual currents and representing an integration of a number of fine-scale movements. Accordingly, a smaller or larger ϵ would be suitable for these options, respectively.

Passive particle tracking runs were conducted to evaluate the computational accuracy of passive movement between a smaller (1-hour) and larger (12-hour) timestep. Metrics of migrations (section 'Metrics of modelled migrations') were similar between the two timesteps, with differences between years much greater than differences between timestep lengths. The computational efficiency of the model is linearly related to the size of the timestep and is decreased by using the hourly rather than the daily SSW-RS files.

This left us with two distinct sets of options: a small timestep δt, with a small ϵ, forced by the hourly SSW-RS files; or a larger δt and ϵ, forced by the daily SSW-RS files. As our focus in this study is the larger-scale migration of post-smolts towards the Norwegian Sea, we chose the second set of options, using a timestep of 12 hours ($\delta t = 43200$ s) with the daily SSW-RS files. This choice allowed for increased computational efficiency, making it possible to simulate a large number of migrations over a number of years. The choice of ϵ could then be made: estimating that our simulated post-smolts would travel between 20 and 40 km/day (in line with tracking studies), then for a 12-hour timestep, a value of $\epsilon = 10$ km is suitable. Additionally, a radius of $\epsilon = 10$ km resolves slightly larger scale salinity patterns (Fig. 3), which might be important for the long-distance marine migration of post-smolts.

We note that there are differences in the temporal and spatial scales between modelled behaviour here and real instantaneous swimming behaviour. These differences mean that the mechanisms modelled in this study do not necessarily represent the exact navigational behaviours employed by post-smolts at each point in time; rather, the model represents an integration of the swimming behaviour and gives a sense of its consequences. While this is suitable for this work, a different approach would be required to simulate fine-scale movements. An alternate version of the model, reserved for future work, would focus on the near-coastal portion of the migration, including tidal currents, and sub-tidal-timescale behavioural decisions.

Particle releases

A group of 21 managed salmon rivers in Scotland, Northern Ireland, and Ireland were selected as the initial particle release locations for the model (Fig. 1), as we expect that they have a qualitatively similar migration route (meaning they have the potential to be represented by a single migration model): we expect that post-smolts from these rivers must cross the continental shelf in a west/northwest direction and then continue northeast along the shelf edge. This group of rivers forms a geographically bounded region, making them a suitable choice for investigating the impact of year-to-year changes in environmental conditions on migrations. Additionally, Tyldesley et al. (2024) found similarities in the marine survival rates of salmon from rivers in this region, suggesting they experience similar marine conditions. Other rivers were tested in the model development process (e.g. rivers on the east coast of Ireland) but it was found that different models would be required for rivers outside this group, and this further generalization is left for future work.
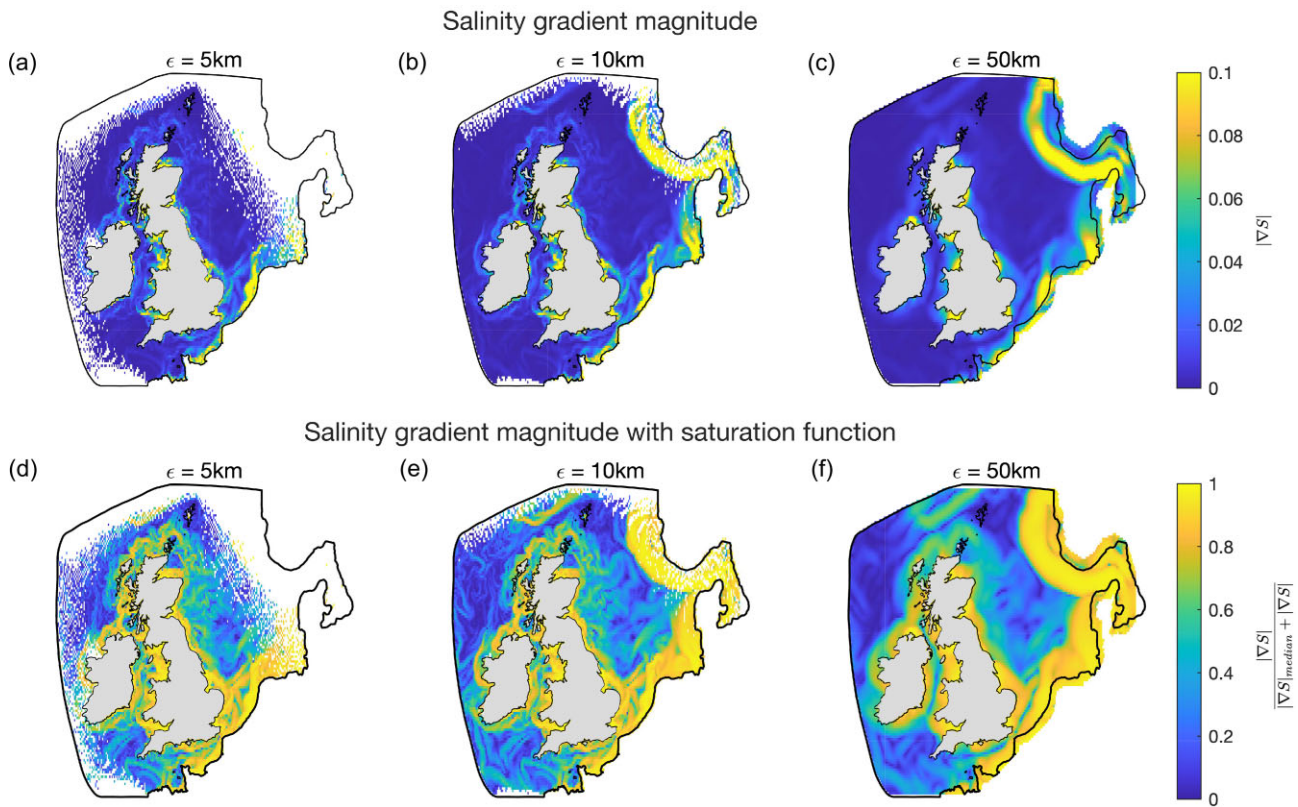
Salinity gradient magnitude

Salinity gradient magnitude with saturation function

Figure 3. Salinity gradient magnitude calculated with: (a) $\epsilon = 5$ km, (b) $\epsilon = 10$ km, and (c) $\epsilon = 50$ km. (d)–(f) show the same salinity gradient magnitude with $\epsilon = 5$km, $\epsilon = 10$km, and $\epsilon = 50$km, respectively, but with the saturation function in the Equation (4) for $\mathbf{g_s}$ applied.

Table 1. Mean 25th and 75th percentile Atlantic salmon (*S. salar*) smolt migration timing from six monitored rivers around the British Isles (https://doi.org/10.5063/F1HQ3XD1 Diack 2021). River numbers are provided for the Burrishoole and the Bush, as displayed in Fig. 1.

River	Latitude	25th percentile date	75th percentile date
Tamar	50.4°	17th April (mean 2005–2019)	26th April
Frome	50.7°	15th April (mean 2006–2019)	N/A
Dee	53.4°	30th April (mean 1997–2019*)	5th May
Burrishoole (15)	53.9°	2nd May (mean 1993–2019)	13th May
Bush (10)	55.2°	28th April (mean 1993–2019)	9th May
North Esk	56.8°	28th April (mean 1993–2013)	9th May

*Data were not available 1998–2000 and 2002–2003.

Smolt migration timing data were available for two of the rivers displayed in Fig. 1 (the River Bush—10, and the Burrishoole—15), and some additional rivers around the British Isles (Table 1). It is known that smolt migration occurs earlier in more southern populations than in more northern populations (Hvidsten et al. 1998, Otero et al. 2014) and it has been seen that river location (described by longitude and latitude) is a key factor in explaining migration timing of smolts (Vollset et al. 2021). Therefore, we estimated the migration timing of the remaining rivers from their latitude. The mean 25th percentile dates (used as a measure for the initiation of migration) were plotted against latitude and a linear model was fitted in MATLAB ($r^2 = 0.61$, $p = 0.06$). Initial particle release times for the 21 rivers were then determined from this model. As seen from the 25th and 75th percentile migration timing, smolt migration from these rivers tends to occur within a short time frame, with the maximum amount of time between 25th and 75th percentile dates per river being 11 days (Table 1). Therefore, to represent the later migrating post-smolts and to act as a sensitivity test, we additionally released particles two weeks later than the initial dates.

A total of 1000 particles were released at each start point per year (500 per release date), corresponding to a total of 567 000 particles released over the 27 years of simulations. All particles were kept at a fixed depth of 5 m (i.e. they were subject to currents at this depth), as post-smolts are generally found at the top of the water column (Renkawitz et al. 2012, Newton et al. 2021). The particle release points were set 30 km away from the river mouths (as seen in Fig. 1), as our focus in this study is on the larger-scale migration behaviour towards the Norwegian Sea and we anticipate that a different scale of modelling would be required for the initial small-scale navigation from the river mouths (section 'Model

timestep'). This additionally helps prevent particle collisions with the coastline.

Growth model

A growth model determined the fork length of simulated post-smolts, as swimming speed depends on body size. We used the growth model of Ounsley et al. (2020), adapted from Mork et al. (2012). This model was derived from the body lengths of seven post-smolts captured in the Northeast Atlantic in 2008 and 2009 (Mork et al. 2012). The fork length of simulated post-smolts in metres was:

$$L = L_0 e^{\alpha d} \tag{7}$$

where L_0 is the initial fork length of the fish in metres, $\alpha = 0.0059$ and d is the number of days spent at sea.

The initial fork length of fish L_0 was based on observation. Scottish smolts range in fork length from 10 to 15 cm, with the mean lying approximately at the middle of this range (Malcolm et al. 2015). However, in the river Bush in Ireland, the mean fork length of migrating smolts from 2017 to 2019 was 14.5 cm (Agri-Food and Biosciences Institute, unpublished data). Nearby, in the river Burrishoole in Ireland, the mean fork length from 1993 to 2020 (the time period of our modelling work) was 13.8 cm (de Eyto and McGinnity 2023, Rinaldo et al. 2023, additional unpublished data). Based on these values, we conservatively set the initial fork length of fish (L_0) from Scottish and Irish rivers to 13 cm ($L_0 = 0.13$ m).

Metrics of modelled migrations

To describe the movement patterns of the modelled migrations, three metrics were calculated:

(1) Proportion of time spent in shallow water (< 200 m) vs deeper water. A depth of 200 m was selected for this metric because it lies on the boundary of the northwest European continental shelf edge (Simpson and Sharples 2012).
(2) Speed relative to the ground (km/day).
(3) Domain exit rate, calculated as the proportion of particles passing through a region at the top of the Scottish Shelf Model domain of depth 50 km, stretching from $-12°$ to $5°$ longitude, within 100 days of entering the sea (i.e. exiting the SSM domain and heading towards known feeding grounds in the Norwegian Sea within an appropriate time frame).

The time of 100 days used for the domain exit rate means that smolts entering the sea at the end of April, for example (Table 1) must reach the Norwegian Sea by early August at the latest. This aligns with observations of post-smolts in the Norwegian Sea in June, July, and August (Gilbey et al. 2021). This choice of time frame might be generous, given it seems that high numbers of post-smolts have already reached the Norwegian Sea by June (Gilbey et al. 2021), but trawling in their study did not extend as far south as the top of our modelling domain in July and early August, so there is no evidence to suggest that post-smolts are not still migrating northwards during this time.

Parameter optimization and sensitivity

The parameters w_c, w_s and w_d, which represent the relative use of each navigational cue, could not be based on empirical values, as the exact navigational mechanisms of salmon are not yet known. Precise values of post-smolt marine swimming speeds in body lengths per second are also not known for this region. Therefore, the parameters w_c, w_s and s were optimised with respect to the domain exit rates (i.e. we developed a model that maximised the number of simulated post-smolts reaching the Norwegian Sea within an appropriate time frame). The speed relative to the ground of simulated migrations was constrained to be no more than 40 km/day, in line with estimates of post-smolt swimming speeds in this region (Lilly et al. 2023). The parameter w_d was determined by the relationship $w_c^2 + w_s^2 + w_d^2 = 1$. To minimize computational time, only 20 particles were released from six rivers (numbers 2, 4, 6, 10, 15, and 19 in Fig. 1), over the years 1993, 2003, 2007, 2012, and 2018 (selected as they display a range of salinity conditions in the SSW-RS domain). Values of w_c and w_s from 0 to 1 were tested at 0.1 resolution. Values of s from 3 to 7 were tested at 0.5 resolution. This equated to a total of 810 parameter combinations tested.

The optimal parameters were $w_c = 0.3$, $w_s = 0.8$ and $s = 5.5$. This gives a value of $w_d = 0.5196$. These parameters were used for the migration simulations across all rivers and years. However, we note that the interannual patterns in domain exit rates were similar for all of the top 10% parameter combinations (Fig. 4a), though the parameters varied (Fig. 4b–c). This suggests that the model results are not highly sensitive to the choice of parameters w_c, w_s and s. We also note that the model produced reasonable domain exit rates for each of the five test years (Fig. 4a), a consistency one would expect in a real evolved behaviour.

The optimization process also allowed us to evaluate whether all three components of the behavioural model **g** were serving an important purpose. When either the salinity gradient-following weight, w_s, or the directional swimming weight, w_d, were set to zero (Fig. 5b–c), domain exit rates were low across years (<0.5). This suggests that these components are key in this model for simulating post-smolt migrations from this group of rivers. Contrastingly, when the current following weight, w_c, was set to zero, domain exit rates were, in some cases, not much lower than the optimal solution (Fig. 5a). However, the variability within years was increased in these cases. The optimal solution, with nonzero w_c, was therefore still deemed beneficial.

A small change in the value of θ_{bias} had only a minor negative impact on the domain exit rates (Fig. 6). An increase in ϵ resulted in a slight increase in domain exit rates, while a decrease in ϵ resulted in a significant decline in exit rates. This suggests that, while following a salinity gradient is beneficial for migration, it must be on the right spatial scale. A larger value of ϵ allows simulated post-smolts to sense conditions over a larger area before deciding on their swimming direction, which might allow a more optimal route to be selected. However, a radius greater than $\epsilon = 10$ km might be unrealistic (section 'Salinity gradient calculation') and Fig. 6 suggests that a larger radius of detection is unnecessary anyway, so our choice of $\epsilon = 10$ km is validated. A small change in the threshold depth at which R in Equation (5) is set to 1 (i.e. the depth at which the directional component is added) had a negative impact on the domain exit rates, suggesting that a behavioural transition is indeed beneficial upon reaching 200 m (or approximately the continental shelf edge).
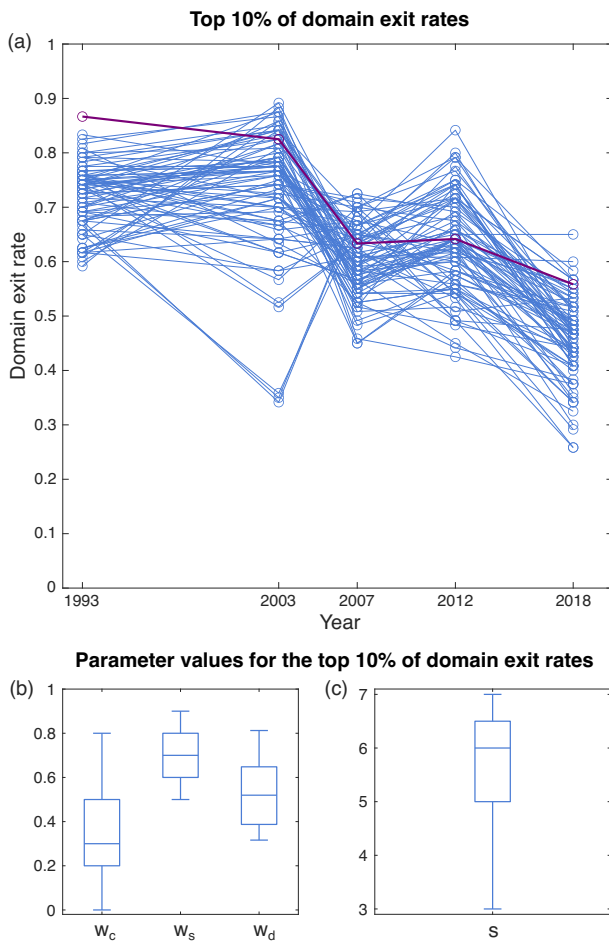
Figure 4. (a) The top 10% of domain exit rates for the parameter optimization runs. The top 10% was determined from the means across each of the 5 years. The optimal solution (greatest mean across the five years) is shown in purple. (b) Boxplots showing the spread of values of parameters w_c, w_s, and consequently, w_d in the top 10% of runs. (c) Boxplot showing the values of s in the top 10% of runs.

Comparing modelled migrations with locations of post-smolts

Observations of salmon migrations (in terms of both position and timing) are very rare on the scale of our study, de-

Figure 6. Changes in domain exit rates when varying the parameters θ_{bias}, ϵ, and the threshold depth at which R is set to 1 (Equation 5) by ±10%.

spite an abundance of acoustic tracking data in coastal and estuarine regions (Barry et al. 2020, Newton et al. 2021, Lilly et al. 2022, 2023, Rodger et al. 2024). Here, we compared our model outputs with the locations of Atlantic salmon post-smolts sampled near the continental shelf edge during the SALSEA-Merge project (http://salmonatsea.com/the-salsea-merge-project/; Utne et al. 2020). Sampling was conducted in 2008 and 2009, but we only used the 2008 data here, due to limited observations within our model domain in 2009. To check both the spatial and temporal overlap of our model output with these observations, we calculated progression along a general migration track for our modelled post-smolts and for the observations. We chose this general migration track to follow the continental shelf edge due to multiple observations of post-smolts at the shelf edge (Shelton et al. 1997, Holm et al. 2000, Utne et al. 2020, Gilbey et al. 2021).

Comparing migration metrics with environmental conditions

Environmental conditions from the SSW-RS were averaged over a region covering the continental shelf west of Ireland and Scotland (i.e. the area relevant to the selected start points for this modelling, Fig. 1) and a similar region covering the shelf edge. These regions were kept separate as they are influenced by different physical processes on different time scales. Conditions were averaged over April to June each year. This period was selected to cover the majority of the modelled
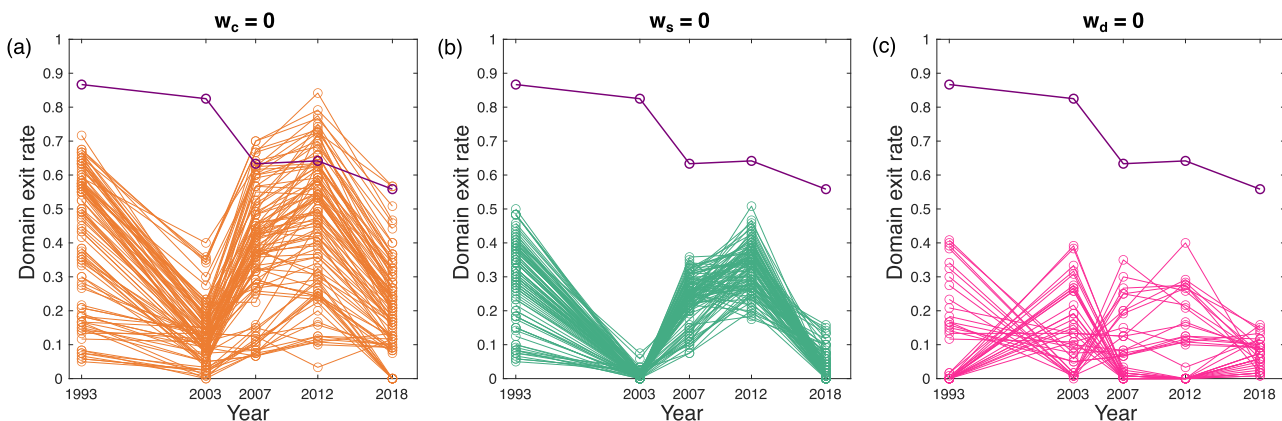

Figure 5. Domain exit rates are displayed for all cases where: (a) $w_c = 0$, (b) $w_s = 0$, (c) $w_d = 0$. The purple line again depicts the optimal solution, in which all weights were nonzero ($w_c = 0.3$, $w_s = 0.8$, $w_d = 0.52$).
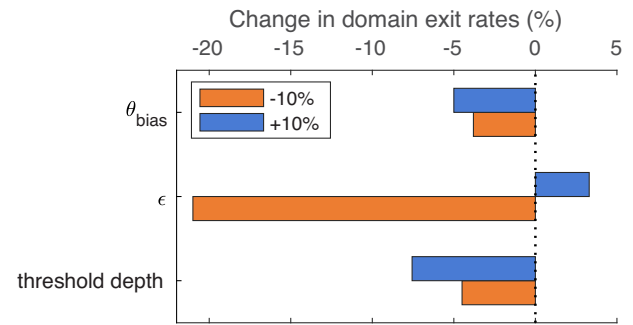
migrations, from particle release dates (section 'Particle releases') to domain exit. While domain exit rates are calculated after 100 days, we expected that many modelled post-smolts will reach the domain exit region earlier than this (with a mean time to exit of 44 days observed in the optimal parameters run in section 'Parameter optimization and sensitivity'), so April to June will cover the key migration period for most simulated post-smolts.

In the on-shelf region, mean surface salinity and mean surface eastward and northward currents were calculated, as we anticipate that these conditions will impact migration from these rivers across the shelf out to the continental shelf edge. In the shelf-edge region, we calculated mean surface salinity, mean surface current velocity at a bearing of 54° (representing along-shelf flow), and the surface current velocity perpendicular to this (representing across-shelf flow; on-shelf positive). A more complex velocity calculation for along- and across-shelf flow in which the coordinate axes precisely followed the terrain gave very similar results. To prevent bias of any of these means due to the greater number of nodes/elements per unit area in some regions of the domain, particularly around the coastlines, the mean of each variable was first taken over 0.5° bins and then the mean of the means was taken.

We also considered variability within the migration period by taking two-week averages from April to June each year of these conditions in both regions. Two-week averages were selected to filter out spring-neap tidal variation and other tidal signals aliased by the 24-hour SSW-RS averages. While the use of tidal currents may be important during the initial, near-shore, migration of post-smolts (e.g. holding position in flow tides and then migrating during ebb tides, Main 2021, Lilly et al. 2022), we expect that residual currents are more important for the remainder of the marine migration (as modelled in this study).

Finally, we considered two indices that describe large-scale climate variability in the North Atlantic and hence might relate to variability in local oceanographic conditions along the post-smolt migration route. We considered the North Atlantic Oscillation (NAO) index (obtained from www.ncei.noaa.gov/access/monitoring/nao/) and the SPG index: several versions of this index are available, but we used that of Hátún and Chafik (2018), which is calculated using principal component analysis of sea surface height; this is seen to be effective in describing water mass variability in the northeastern Atlantic (Koul et al. 2020). As a reanalysis, the SSW-RS encompasses changes to water properties described by changes in the SPG and NAO indices. However, we still find these climate indices of interest on their own, as they might be useful indicators of post-smolt migrations, particularly for years preceding the start of the SSW-RS (1993). The annual mean SPG and NAO indices over our study period are shown in the Supplementary Information. We also considered the mean NAO index over only April-June each year (coinciding with the time period of averaging of the SSW-RS conditions). This time series was included as it provides a more time-specific measure of surface wind forcing (which influences surface currents) in this region. This version of the NAO index follows a similar pattern as the annual mean NAO index, but with greater peaks and troughs.

To consider the potential relationships between environmental conditions (salinity, currents, NAO, and SPG indices) and migrations, all correlations between the metrics for these conditions and the metrics of modelled migrations were calculated. Initially, each combination of metrics was plotted against each other (not shown) to check for any obviously non-linear relationships; none were found. Then, Pearson correlation coefficients (r) were calculated for each combination of metrics, giving a measure of the linear dependence of each of these relationships. Additionally, P-values were calculated for each combination, testing the null hypothesis that there is no relationship between each metric and each environmental condition. Some of the environmental variables display autocorrelation, so the modified Chelton method, where the degrees of freedom are altered based on the level of autocorrelation, was used to calculate stricter P-values (Pyper and Peterman 1998).

Investigating differences in migration metrics between rivers

To consider differences between rivers, two metrics were calculated for each river mouth start point:

(1) The minimum straight line distance from each start point to the continental shelf edge (defined by the 200 m isobath).
(2) The total minimum migration distance, a combination of the above distance and the remaining distance along the continental shelf edge track line (section 'Comparing modelled migrations with locations of post-smolts') to the domain exit.

The relationships between each of these metrics of migration distance and the mean migration metrics of each river were tested by calculating r and P values as above.

Comparing migration metrics with return rates

Modelled domain exit rates per year were compared with a time series of combined normalized marine return rates of one-sea-winter (1SW) Atlantic salmon from five rivers on the west coasts of Ireland, the United Kingdom, and France (Tyldesley et al. 2024). The return rates act as a proxy for marine survival rates, and the rivers include the Bush, Burrishoole, and Corrib (numbers 10, 15, and 17, respectively in Fig. 1). Pearson correlation coefficients and stricter P-values accounting for autocorrelation in the time series were calculated as detailed in section 'Comparing migration metrics with environmental conditions'. Additionally, these correlation coefficients were calculated between modelled domain exit rates and detrended return rates ($r_{detrend}$, $p_{detrend}$), where the time series were detrended by subtracting the mean value from each data point.

Results

Modelled migrations

Most modelled migrations followed a common route along the continental shelf edge. However, some modelled post-smolts were found outside this common route in the Irish Sea and the Celtic Sea (Fig. 7). Any particles passing through the defined domain exit region were removed from the simulations. Domain exits were concentrated in a small region (Fig. 7), which aligns with the continental shelf edge, suggesting simulated post-smolts stay in the shelf-edge current.

Spatial concentrations of simulated post-smolts for each year of simulations are additionally provided in Supplementary Information. Some differences in distributions
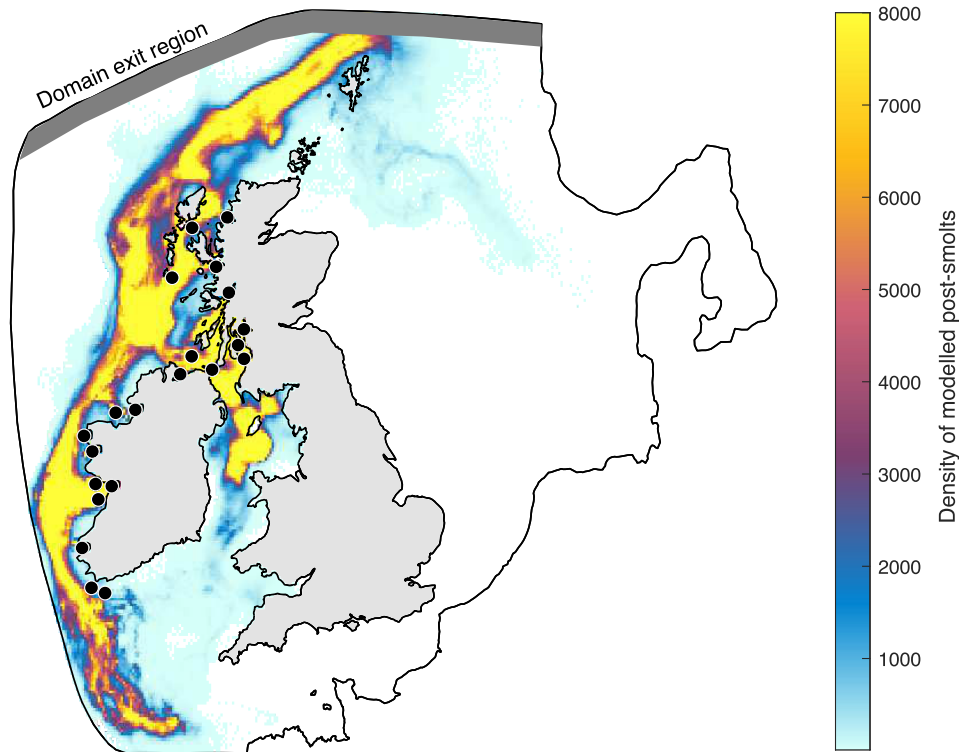
Figure 7. Density of modelled Atlantic salmon post-smolts (*S. salar*) from all releases of all years, measured as the total number of incidences of particles per 30 km² bin. Modelling start points (river mouths) are shown as black circles. The domain exit region, used for calculating domain exit rates, is also displayed.

were seen between years. For example, there was a concentration of particles south of Ireland (in the Celtic Sea) in some years but not others (e.g. 2002 but not 2008). In some years there was also a concentration of particles in the northern North Sea (e.g. 2017 but not 2016).

The modelled distribution of post-smolts was mainly consistent, spatially and temporally, with observations of post-smolts from the SALSEA-Merge project in 2008 (Fig. 8). There was greater overlap, both spatially (Fig. 8a and b) and temporally (Fig. 8b) with the lower latitude observations, which lie close to the continental shelf edge.

Variability in environmental conditions and migrations

Both on the shelf and at the shelf edge, conditions from April to June varied between years (Fig. 9). Surface salinity on the shelf was lower than at the shelf edge, but interannual variability was seen in salinity across both regions. Surface currents also varied significantly between years both on the shelf and at the shelf edge.

Among 2-week periods in April-June, salinity was variable in the shelf region, while it was fairly consistent within years at the shelf edge (Fig. 9a and d). Currents were highly variable between the 2-week periods, both on the shelf and at the shelf edge (Fig. 9b, c, e, and f).

Metrics of modelled migrations varied both between years and between rivers (Fig. 10). The proportion of time spent in water of depth <200 m was very high (>0.9) across all rivers in some years (e.g. 2002–2004), while in other years

it was more variable between rivers. In addition, some rivers had high values (>0.8) of this metric across most years (e.g. rivers 6–8 and 20–21: Leven, Glenmore, Ayr, Owenreagh, Coomhola). The mean metric per year across all rivers ranged from a minimum of 0.81 in 2016 to a maximum of 0.98 in 2003 and 2017.

Speeds of modelled migrations also varied between years and rivers (Fig. 10c and d). Some rivers had noticeably high or low speeds across most years: rivers 6–8 (Leven, Glenmore, Ayr) displayed fairly fast speeds (>25 km/day) across all years, coinciding with a high proportion of time spent in shallow water (Fig. 10a). Contrastingly, rivers 20 and 21 (Owenreagh and Coomhola) showed lower speeds (∼20 km/day) across years, while also spending a high proportion of time in shallow water. Migration speeds were highly variable across years: the mean speeds ranged from a minimum of 22.6 km/day in 2001 to a maximum of 33.4 km/day in 2012.

Domain exit rates showed significant variation between rivers and between years (Fig. 10e and f). Across rivers, particularly low rates (∼0.25) were seen across the period for rivers 6–8 and 20–21, the same group of rivers that spent high proportions of time in shallow water. Other rivers maintained high exit rates (>0.7) in most years (e.g. rivers 1–4: Bharp, Mhuil, Ullapool, and Arnisdale). The mean domain exit rate (mean across rivers per year) ranged from a minimum of 0.15 in 2017 to a maximum of 0.73 in 2008. There was a weak declining trend in the domain exit rates over the study period (mean change of −0.007 per year, $r^2 = 0.166$, $P = 0.03$).
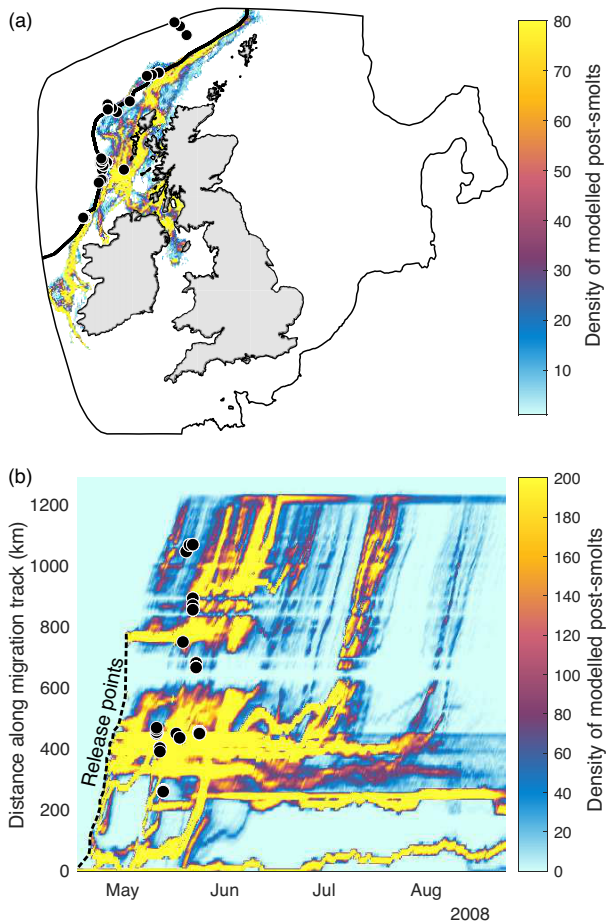
Figure 8. (a) Simulated Atlantic salmon post-smolt (*S. salar*) density (total number of particles per 30 km² bin) from 2008 within ± 1 week of all observations from the SALSEA-Merge project (http://salmonatsea.com/the-salsea-merge-project/; Utne et al. 2020), which are marked as black dots. The general migration track following the continental shelf edge is shown as a black line. (b) Distance along this general migration track with time for simulated post-smolts and observations, again marked as black dots. The black dashed line displays particle release locations and timing.

There were only minor differences in the migration metrics between the earlier and later releases (Fig. 10b, d, and f), with much greater variability between years than between releases.

Mechanisms behind variability in migrations

Correlations between the on-shelf and shelf-edge SSW-RS conditions, NAO and SPG indices, and the migration metrics are shown in Fig. 11.

On the shelf, both surface salinity and currents influenced modelled migrations. On-shelf salinity and eastward currents were both significantly negatively correlated to the speed of migrations, while eastward currents were also positively correlated with the proportion of time spent in water <200 m deep (Fig. 11a and d). Northward currents on the shelf were positively correlated to domain exit rates.

At the shelf edge, surface salinity had no clear impact on modelled migrations (Fig. 11b and d). Surface currents perpendicular to the shelf edge were positively correlated to the proportion of time spent in water <200 m deep, while currents along the shelf edge were negatively correlated to this

metric. Similarly, currents perpendicular to the shelf edge were negatively correlated to the speed of migrations, while currents flowing along the shelf edge were positively correlated to speed.

The April-June mean NAO index was positively correlated to the proportion of time spent in water <200 m deep (Fig. 11c and d). While the SPG index was not directly correlated to the migration metrics, it was significantly correlated with shelf and shelf-edge salinity. The April-June NAO index was additionally correlated with shelf and shelf-edge currents, which are themselves correlated with the speed of modelled migrations and the time spent in water <200 m deep.

Differences between rivers

The minimum distance from each river start point to the continental shelf edge and the total minimum migration distance from each river were both correlated to the proportion of time spent in shallow water and the domain exit rate (Table 2). Neither of these distances were correlated to the speed of migrations.

Comparison between marine return rates and modelled migrations

There was weak evidence (at the 90% confidence interval, $P < 0.1$) of a correlation between 1SW marine return rates and the modelled domain exit rates (Fig. 12). This correlation did not hold when the time series were detrended ($P_{detrend} > 0.1$).

Discussion
Migration model

We developed a post-smolt migration model combining three mechanisms: following local currents, following the local salinity gradient, and directional swimming. The behavioural model developed in this study may not exactly represent the real instantaneous swimming behaviour of post-smolts, as the spatial and temporal scales in the model are greater than those used for real instantaneous navigation. However, it gives a representation of migrations that shows good agreement with limited observational data (Fig. 8). This representation allows us to consider interannual variability in migrations and the mechanisms driving this.

All three of the behavioural components considered were found to be beneficial in terms of domain exit rates (Fig. 4), meaning they resulted in a model where simulated post-smolts exited our domain in high numbers within a time that was in line with trawling studies in the Norwegian Sea (Gilbey et al. 2021). We also found that reasonably high domain exit rates could be obtained when omitting the current-following behaviour (Fig. 5a). This suggests that currents might be less important as an active swimming cue than the salinity gradient-following and directional swimming behaviours. This agrees with the findings of Newton et al. (2021), who found that post-smolt swimming direction was not explained by the current direction, and Ounsley et al. (2020), who found that post-smolt migrations from around Scotland could not be simulated with only a current-following behaviour. This result might not hold universally, however, given that other studies have indeed found evidence of post-smolts using currents to guide their migration (e.g. Lilly et al. 2022). Additionally, even if ocean currents are not used as an active
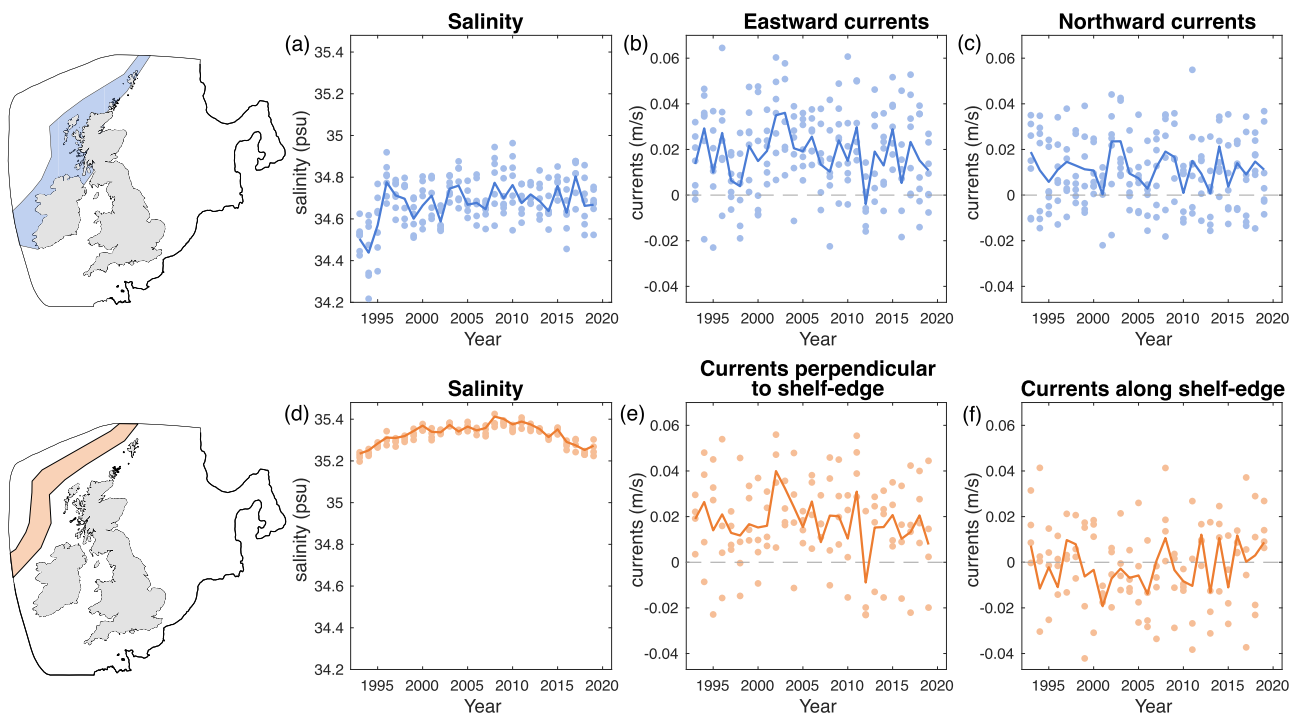
Figure 9. Scottish Shelf Waters Reanalysis Service (SSW-RS) conditions averaged over April–June each year for the shelf region (blue) and the shelf-edge region (orange): (a) shelf salinity; (b) shelf eastward currents; (c) shelf northward currents; (d) shelf-edge salinity; (e) currents along the shelf edge; (f) currents perpendicular to the shelf edge (on-shelf positive). Lines show conditions averaged over 1st April to 30th June each year. Dots show conditions averaged over 2-week periods from 1st April to 24th June.

swimming cue, they will still passively influence post-smolt migrations.

Comparison with locations of post-smolts

The spatial and temporal overlap of our modelled distributions of post-smolts with observations of post-smolts from the SALSEA-Merge project (Fig. 8) suggest that our movement model can describe post-smolt migrations in this region to a reasonable accuracy. However, the observations from the SALSEA-Merge project are not comprehensive, and, crucially, they do not provide information on where post-smolts were not found. Additionally, comparisons between our modelled migrations and the observations must be interpreted cautiously as we do not know the rivers of origin of the observed post-smolts and there are likely to be differences in migration routes and timings between stocks (though some post-smolts captured in this region have been genetically assigned to British/Irish origin; Gilbey et al. 2021). There are also likely to be significant differences in migration patterns between years, but we could only compare with observations from one year (2008) of our 27-year study period.

Modelled distributions of post-smolts

Most modelled migrations followed a route along the continental shelf edge (Fig. 7), which is consistent with multiple observations of post-smolts in the shelf-edge current (Shelton et al. 1997, Holm et al. 2000, Utne et al. 2020, Gilbey et al. 2021). However, given the highly variable conditions that force modelled movement, plus the stochastic element of movement, we did not expect to see all modelled migrations taking exactly the same route. Instead, we found

variation in paths both within and between years (Fig. 7 and Supplementary Information). Some simulated post-smolts from rivers 6–9 travelled south into the Irish Sea (Fig. 7), which explains the low domain exit rates seen for these rivers (Fig. 10). Similarly, some post-smolts from rivers 20 and 21 (Owenreagh and Coomhola) travelled south into the Celtic Sea in some years (e.g. 2002). This agrees with the findings of Mork et al. (2012), who simulated post-smolt migrations in this region in 2002 and 2008 and found a concentration of post-smolts south of Ireland in 2002, but not in 2008.

The low domain exit rates and southwards direction of travel observed here for rivers 6–9 and 20–21 might suggest that post-smolts from these rivers have to utilize a different behaviour or navigational cue in their initial marine migration, in which case a different model would be required to simulate their migrations. Further work could investigate the application of different behavioural models to these rivers, for example, using a different threshold for the inclusion of the directional component, or a different bearing for the directional component.

Variable migrations

The differences in migration trajectories between years shown in the Supplementary Information relate to differences in the metrics of migrations. For example, in 2015 there was a greater concentration of simulated post-smolts distributed across the shelf than in 2016, relating to a larger proportion of time spent in shallow water in 2015 (0.98) than in 2016 (0.84). This metric was high (>0.8) across all years, indicating that the majority of each modelled migration was spent on the shelf and that the overall speed of migrations was faster once off the shelf (this result is at least in part caused by the
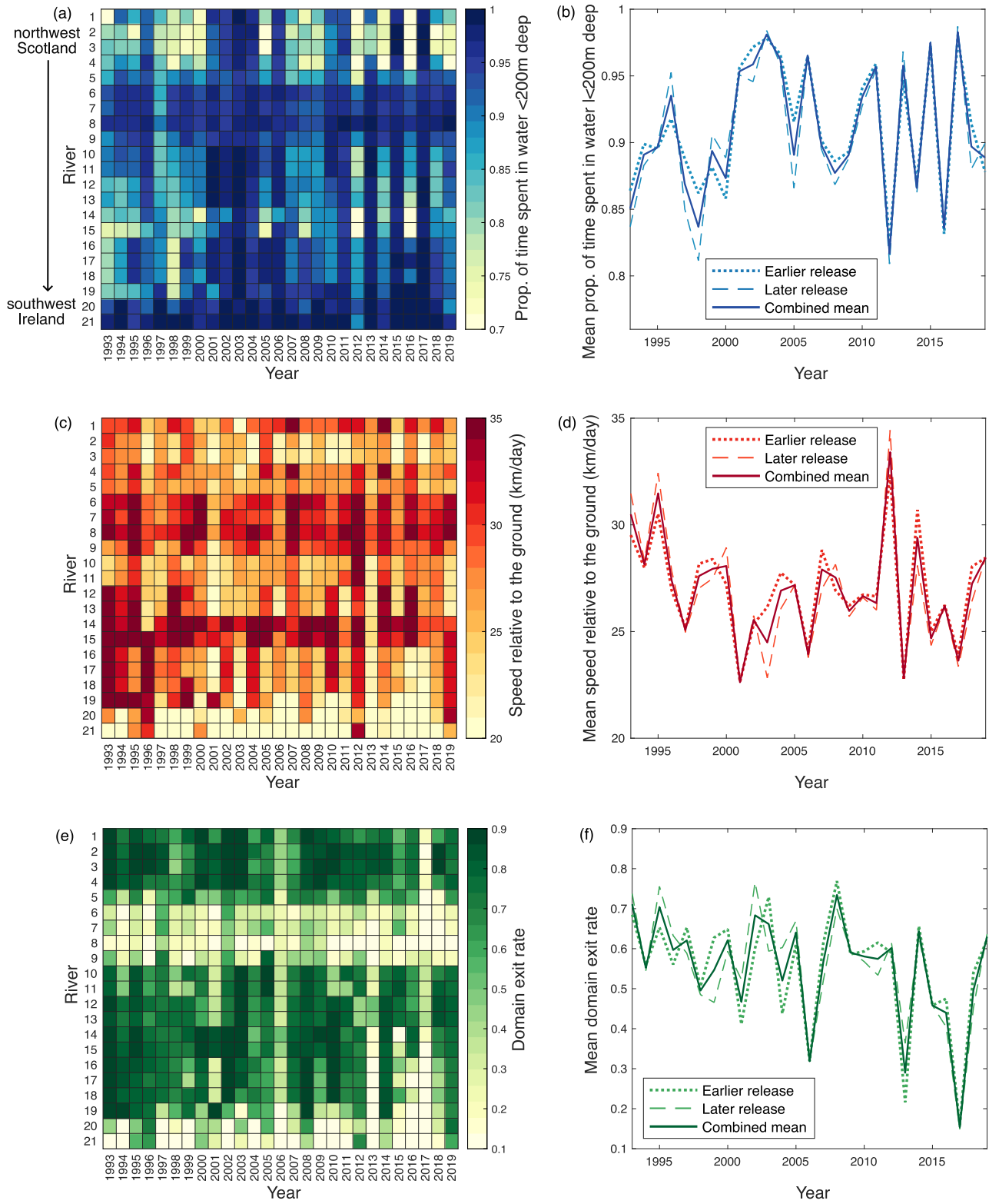
Figure 10. (a), (c), (e): Heatmaps displaying metrics of modelled Atlantic salmon (*S. salar*) migrations per river per year (including both releases). (b), (d), (f): Metrics of modelled migrations (mean taken across rivers) for the earlier and later (2 weeks later) particle releases, and the combined mean (both releases).

addition of the directional component at a depth of 200 m). At present, there is unfortunately no empirical data with which to compare the modelled proportion of time spent on the shelf. Physical conditions differ between the continental shelf and

the shelf edge (Fig. 9) and biological conditions, such as prey and predator fields, are also likely to differ between the on and off-shelf regions (Simpson and Sharples 2012). This suggests that year-to-year changes in the proportion of time spent in
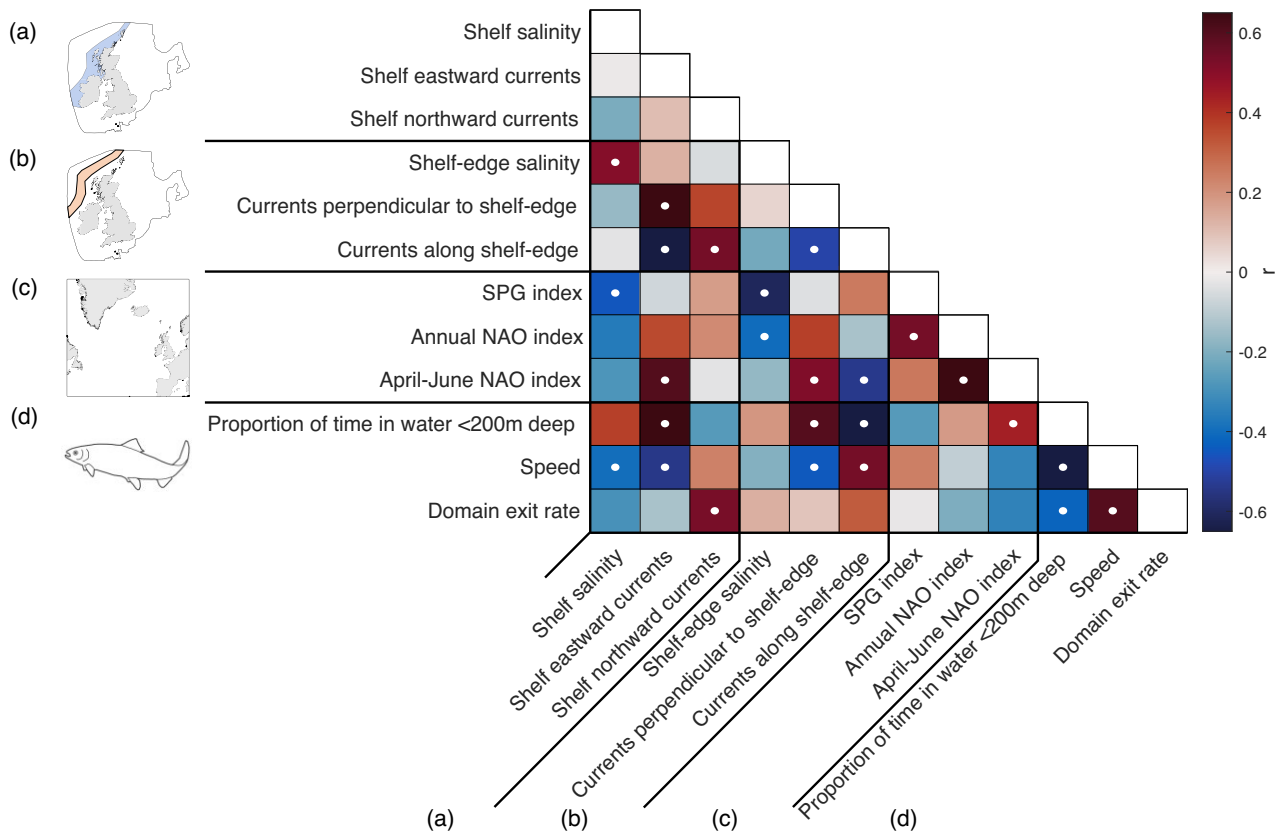
Figure 11. Correlation matrix between: (a) on-shelf salinity and currents, (b) shelf-edge salinity and currents, (c) large-scale climate indices (subpolar gyre SPG and North Atlantic Oscillation NAO), (d) modelled Atlantic salmon (*S. salar*) migration metrics. Pearson correlation coefficients (*r*) between each combination are shown via the colour scale. Significant correlations ($P* < 0.05$) are denoted by white dots.

Table 2. Linear relationships between the mean migration metrics per river and the minimum distance from each river to the continental shelf edge, or the total minimum migration distance.

	Proportion of time in water <200 m deep	Speed relative to the ground	Domain exit rate
Minimum distance to continental shelf edge	$r^2 = 0.381$, $P = 0.003$	No correlation	$r^2 = 0.677$, $P < 0.0001$
Total minimum migration distance	$r^2 = 0.561$, $P < 0.0001$	No correlation	$r^2 = 0.271$, $P = 0.02$
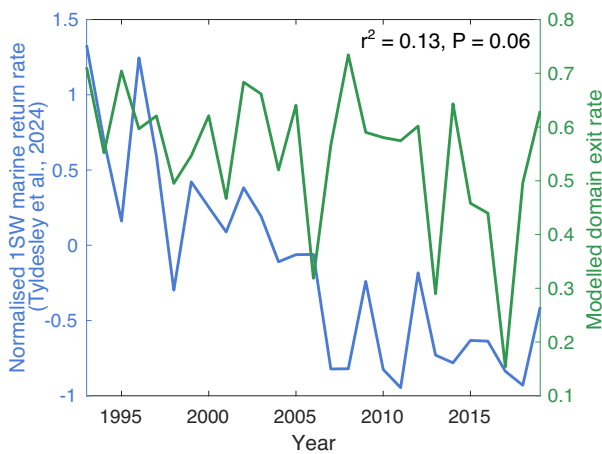
Figure 12. Time series of grouped 1SW normalized return rates from western populations (blue line; Tyldesley et al. 2024; normalization was by z-scores across whole time series, 1980–2019) and modelled domain exit rates (green). Correlation coefficients between the time series are shown.

shallow water could result in changes in the physical and biological conditions experienced by post-smolts during their early marine migration, influencing growth and survival. If prey conditions are richer on the shelf, then spending a large proportion of time on the shelf could be beneficial to post-smolts, or vice versa.

Mean domain exit rates ranged from 0.15 to 0.73 between years (Fig. 10). This variation shows that modelled migrations are highly influenced by interannual changes in environmental conditions. While the domain exit rates might not directly correlate to the 'success' or survival of real post-smolts, these rates might still suggest years in which migration might be easier (higher domain exit rate) or harder (lower domain exit rate). If the interannual variability in the domain exit rates of our modelled migrations is greater than the variability in real post-smolt migration success during this time, this may suggest that post-smolts can adapt their migratory behaviour between years to deal with changes in conditions, as concluded by Burke et al. (2016) for juvenile Pacific salmon migration.

It is hard to draw comparisons between our model results and the marine survival rates of Atlantic salmon for two main reasons: first as we did not include any mortality in our modelling, and second as we only modelled migrations over the first 100 days at sea, while most Atlantic salmon will spend 1–4 years at sea (Aas et al. 2010). However, there was some evidence of a weak relationship between marine return rates and modelled domain exit rates (Fig. 12), which have both declined over the study period. This might suggest that the declining success (or increasing difficulty) of post-smolts reaching their summer feeding grounds might be one factor driving declines in marine survival. However, detrended marine return rates were not significantly correlated with modelled domain exit rates, so interannual fluctuations in modelled migrations are not synchronous with fluctuations in marine survival rates.

Speeds of up to 33.4 km/day were seen in our modelled migrations. These are in line with rapid post-smolt migration speeds measured recently in the Irish Sea of up to 39.9 km/day (Lilly et al. 2023), and speeds of up to 53.8 km/day measured to the west of Scotland (Rodger et al. 2024).

In addition to the interannual variation in modelled migrations, we also saw differences between rivers (Fig. 10). This is in line with the findings of Rodger et al. (2024), who saw differences in migration paths and speeds between rivers. We found that between-river differences in domain exit rates were related both to their minimum distance from the continental shelf edge and to their total minimum migration distance (Table 2). This is in line with the finding of Lilly et al. (2023), who saw that the minimum migration success of post-smolts in the Irish Sea (based on receiver detections of acoustically tagged fish) was correlated with their minimum distance of travel (from river of origin to the marine arrays). Here, the minimum distance from each river to the shelf edge explained 68% of the between river variation in domain exit rates, while the total minimum migration distance explained only 21% (Table 2). This might suggest there are greater navigational challenges in the first section of the marine migration (i.e. from the coastline out to the continental shelf edge) than the rest of the journey (following the continental shelf edge towards the Norwegian Sea).

Environmental variability and its relation to variability in migrations

Both within and between years, surface salinity was highly variable on the shelf (Fig. 9a). Wind-driven changes influence the propagation of freshwater from the coastline across the shelf west of Ireland and Scotland and the transport of higher-salinity Atlantic water onto the shelf, causing such variability in salinity (Jones et al. 2018, Barton et al. 2024). At the shelf edge, we found that salinity was much less variable, and the magnitude of variability was greater between, rather than within, years (Fig. 9d).

The shelf-edge current was highly variable between years (Fig. 9e and f). We found that stronger currents perpendicular to the shelf edge (on-shelf positive) caused an increased amount of time to be spent in shallow water (i.e. it was harder for the simulated post-smolts to reach or remain at the shelf edge or in deeper water), while stronger currents along the shelf edge reduced the amount of time spent in shallow water (Fig. 11). Therefore, years with stronger, or more directed, currents along the shelf edge might allow for a faster or eas-

ier migration. These relationships are in line with the findings of Moriarty et al. (2016) that variability in surface currents is related to variability in post-smolt migrations.

We expected that the within-year variability in the shelf-edge current (Fig. 9e and f) might also have a significant impact on migrating post-smolts: the differences between two-week periods could mean that post-smolts leaving their rivers earlier or later experience different currents at the shelf edge, which could lead to different outcomes to their initial marine migration. However, we found that the metrics of modelled migrations were similar across our two release dates (Fig. 10), which suggests that the date of commencing migration is less important than the differences in conditions between years.

While we did not find a significant difference in modelled migration metrics between the two release dates (Fig. 10), we anticipate that a change in migration timing has impacts stretching beyond those conveyed by our results. The timing of prey availability is an important factor in the survival and recruitment of fish populations (Cushing 1990), and in anadromous salmonids it is vital that the timing of migration coincides with the timing of sufficient prey availability (Satterthwaite et al. 2014, Wilson et al. 2021). Therefore, while a two-week difference in migration timing had only a minor impact on the outcome of modelled migrations, this change might have a greater effect on the real growth or survival rates of post-smolts.

Surface salinity on the shelf was negatively correlated with the speed of migrations (Fig. 11a and d). This suggests that years with lower on-shelf salinity might have a larger, or more directed, salinity gradient. Therefore, if post-smolts indeed use salinity as a cue to guide their migration, they might be able to migrate more quickly or easily in lower salinity years.

The SPG index was negatively correlated to salinity on the shelf and at the shelf edge. These relationships are expected: it is known that variability in the shelf-edge current is related to changes in the strength of the SPG (Marsh et al. 2017, Clark et al. 2022). Given that salinity (on-shelf and shelf edge) and shelf-edge currents were seen to influence modelled migrations (Fig. 11a/b and d), we expect that the strength of the SPG will have an indirect effect on migrations. Similarly, the April-June NAO index was correlated to shelf and shelf-edge currents, suggesting it will influence migrations. This agrees with the finding of Mork et al. (2012) that modelled migrations differed between a positive NAO year (2002) and a negative NAO year (2008). Based on the correlations found between environmental conditions and metrics of modelled migrations (Fig. 11), a summary of the beneficial oceanographic conditions for simulated post-smolt migrations is provided in Fig. 13.

We have seen that changes in local salinity and surface currents, and changes described by the SPG and NAO indices, can physically influence post-smolt migrations, regarding the path taken or the time taken to migrate, but these changes likely have further impacts on post-smolts. Shifts in water masses related to a stronger SPG have been related to an increase in the abundance of *Calanus finmarchicus* and other copepods in the northeast Atlantic (Hátún et al. 2009), key species in the energy transfer from phytoplankton to forage fish, of which the larvae are a prey item of post-smolts (Utne et al. 2021). Similarly, negative phases of the NAO have been related to increased *Calanus finmarchicus* abundance in the northeast Atlantic (Greene and Pershing 2000, Drinkwater et al. 2003). Changes in zooplankton energy such as the above
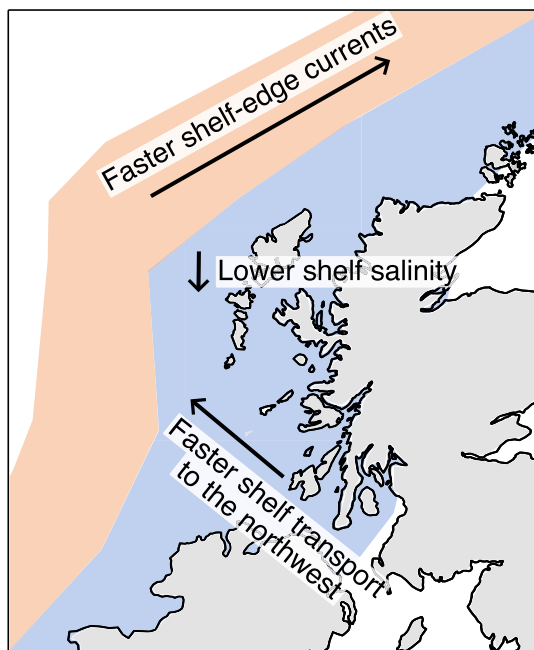
Figure 13. A summary of the beneficial oceanographic conditions for simulated Atlantic salmon (*S. salar*) post-smolt migrations, based on the correlations displayed in Fig. 11. Faster shelf-edge currents and faster on-shelf northwest currents are both associated with a negative North Atlantic Oscillation (NAO) index. Lower on-shelf salinity is associated with a stronger SPG index.

have been related to salmon return rates within our study region (Tyldesley et al. 2024). Given we found that the beneficial oceanographic conditions for post-smolt migrations in this study (Fig. 13) were associated with a negative NAO index and a strong SPG index (Fig. 11), these relationships suggest that good prey conditions for post-smolts might occur concurrently with good physical migration conditions.

Our finding that a negative NAO phase relates to beneficial physical ocean conditions for migrations is in line with the negative correlation found between the NAO index and salmon marine survival from the rivers Burrishoole and Corrib (river locations displayed in Fig. 1, Peyronnet et al. 2008). Contrastingly, Jonsson and Jonsson (2004) found a positive relationship between the NAO index and salmon growth during the first year at sea for a Norwegian river. This highlights the potential differences in the effects of variable environmental conditions across different regions and emphasizes the need to focus on underlying mechanisms driving changes in growth and survival.

At present, there is a lack of empirical data on post-smolt migrations. This means that aspects of our work remain uncertain, and we hope that future advances and new data sources (e.g. in telemetric methods or trawling studies) will help clarify our results. The precise migration paths of post-smolts cannot be predicted by our model, nor can we say that our model represents the exact navigational cues used by post-smolts (especially as our modelling is on a larger spatial scale than instantaneous navigation). While we have evaluated the direction of response of the migration metrics to various changes in environmental conditions, the scale of variability in migration metrics among rivers and years is still uncertain, particularly as our model did not include mortality. Additionally, despite the optimization process applied

to develop our behavioural model, it is still difficult to say exactly which environmental cues are used to 'signpost' post-smolt migration. Future surface trawling or marine telemetry studies for post-smolts should consider the oceanographic conditions both at the known locations of post-smolts and in nearby locations where post-smolts were not observed. This might provide a better idea of the potential choice of environment by post-smolts, as well as providing further basis to the behavioural decisions made in future modelling work.

Despite these uncertainties, our work has revealed that particular oceanographic conditions are beneficial for post-smolt migrations and that changes in these conditions might explain some year-to-year variability in migrations. We also found that differences in migration metrics between rivers were well explained by their distance to the continental shelf edge, which agreed with the findings of a recent telemetry study in the same area (Lilly et al. 2023). Our results are of value in marine spatial planning, for example, evaluating the potential overlap between migrating post-smolts and offshore energy developments, fisheries, and aquaculture sites. Further development of this migration model will offer better integration of the variable opportunities and risks associated with feeding, growth, and predation along and between migration corridors. These results can be used to improve the quality of salmon-focused ecosystem assessments (Bull et al. 2022) and develop predictions for future marine survival chances.

Conclusion

This study modelled interannual variation in Atlantic salmon post-smolt migration pathways from Scottish and Irish rivers over 27 years. We developed an active swimming model in which post-smolts utilized ocean currents, salinity, and magnetic cues to guide their migration. The model does not predict the exact paths taken by migrating salmon, but instead it allows us to consider the mechanistic impact of various physical environmental conditions on migrations. We found that migrations varied significantly between years, with metrics of migrations correlated to time series of local surface currents and salinity. Beneficial oceanographic conditions for migrations were found to be low salinity on the shelf, fast northwest currents on the shelf, and fast shelf-edge currents. These conditions are associated with a negative NAO index and a strong SPG index. The physical differences in migrations between years (in the proportion of time spent in shallow water, the speed of migrations, and the domain exit rate) suggest the likelihood of differences in the biological conditions experienced by fish, for example, in the prey fields they might encounter along their migration. Variation in migrations between rivers suggests that post-smolts migrating from different rivers are impacted differently by environmental conditions. Future modelling work could extend this model to be applicable to a larger set of rivers and compare regional differences while still considering the full 27-year period as we have done here. These results could test whether similarities in the outcomes of modelled migrations between groups of rivers relate to groupings in marine return rates or phylogenetic groupings.

Funding

University of Stirling, the Missing Salmon Alliance, and the Fishmongers Company.

Author contribution

A.B.: conceptualization, methodology, analysis, manuscript writing; N.B.: conceptualization, methodology, analysis, supervision; A.G.: methodology, supervision; D.S.: methodology, supervision; E.T.: methodology, supervision; C.B.: conceptualization, methodology, supervision. All authors contributed to manuscript editing.

Supplementary data

Supplementary material is available at the *ICES Journal of Marine Science* online version of the manuscript.

Conflict of interest: The authors have no conflict of interest to declare.

Data availability

The particle tracking software FISCM is available at https://github.com/GeoffCowles/fiscm/tree/ounsley_et_al_2019. The SSW-RS is available at https://doi.org/10.7489/12423-1. Smolt migration timing data is available at https://doi.org/10.5063/F1HQ3XD1. Body lengths of juvenile salmon from the Burrishoole river are available at https://data.gov.ie/dataset/fish-lengths-of-juvenile-atlantic-salmon-from-the-burrishoole-catchment-co-mayo-ireland-1997-2019.

References

Aas Ø, Klemetsen A, Einum S *et al. Atlantic Salmon Ecology*. Oxford, United Kingdom: John Wiley and Sons, 2010.

Allan I, Ritter J. Salmonid terminology. *ICES J Mar Sci* 1977;**37**:293–9. https://doi.org/10.1093/icesjms/37.3.293

Arheimer B, Pimentel R, Isberg K *et al.* Global catchment modelling using world-wide hype (wwh), open data, and stepwise parameter estimation. *Hydrol Earth Syst Sci* 2020;**24**:535–59. https://doi.org/10.5194/hess-24-535-2020

Autret E, Piollé JF, Tandéo P *et al.* European North West Shelf/Iberia Biscay Irish Seas - High Resolution L4 Sea Surface Temperature Reprocessed. Tech. Rep. 1.4 2020. https://doi.org/10.48670/moi-00153 (November 2024, last accessed).

Barry J, Kennedy RJ, Rosell R *et al.* Atlantic salmon smolts in the irish sea: first evidence of a northerly migration trajectory. *Fish Manage Ecol* 2020;**27**:517–22. https://doi.org/10.1111/fme.12433

Barton B, De Dominicis M, O'Hara Murray R *et al.* Scottish Shelf Model 3.02 - 27 Year Reanalysis. 2022. https://doi.org/10.7489/12423-1 (June 2024, last accessed).

Barton BI, De Dominicis M, O'Hara Murray R *et al.* Formation and dynamics of a coherent coastal freshwater influenced system. *Earth Space Sci* 2024;**11**:e2023EA002872. https://doi.org/10.1029/2023EA002872

Bartsch J, Coombs S. A numerical model of the dispersion of blue whiting larvae, *Micromesistius poutassou* (Risso), in the eastern north Atlantic. *Fish Oceanogr* 1997;**6**:141–54. https://doi.org/10.1046/j.1365-2419.1997.00036.x

Bell V, Kay A, Jones R *et al.* Use of soil data in a grid-based hydrological model to estimate spatial variation in changing flood risk across the UK. *J Hydrol* 2009;**377**:335–50. https://doi.org/10.1016/j.jhydrol.2009.08.031

Booker DJ, Wells NC, Smith IP. Modelling the trajectories of migrating Atlantic salmon (*Salmo salar*). *Can J Fish Aquat Sci* 2008;**65**:352–61. https://doi.org/10.1139/f07-173

Bull CD, Gregory SD, Rivot E *et al.* The likely suspects framework: the need for a life cycle approach for managing Atlantic salmon (*Salmo salar*) stocks across multiple scales. *ICES J Mar Sci* 2022;**79**:1445–56. https://doi.org/10.1093/icesjms/fsac099

Burke BJ, Anderson JJ, Miller JA *et al.* Estimating behavior in a black box: how coastal oceanographic dynamics influence yearling chinook salmon marine growth and migration behaviors. *Environ Biol Fish* 2016;**99**:671–86. https://doi.org/10.1007/s10641-016-0508-7

Byron CJ, Burke BJ. Salmon ocean migration models suggest a variety of population-specific strategies. *Rev Fish Biol Fish* 2014;**24**:737–56. https://doi.org/10.1007/s11160-014-9343-0

Byron CJ, Pershing AJ, Stockwell JD *et al.* Migration model of post-smolt Atlantic salmon (*Salmo salar*) in the gulf of maine. *Fish Oceanogr* 2014;**23**:172–89. https://doi.org/10.1111/fog.12052

Chapman BB, Hulthén K, Wellenreuther M *et al.* Patterns of animal migration. *Animal Movement Across Scales*. Vol. **1**. Oxford, United Kingdom: Oxford University Press, 2014, 11–35. https://doi.org/10.1093/acprof:oso/9780199677184.003.0002

Chen C, Liu H, Beardsley RC. An unstructured grid, finite-volume, three-dimensional, primitive equations ocean model: application to coastal ocean and estuaries. *J Atmos Ocean Tech* 2003; **20**:159–86.

Clark M, Marsh R, Harle J. Weakening and warming of the european slope current since the late 1990s attributed to basin-scale density changes. *Ocean Sci* 2022;**18**:549–64. https://doi.org/10.5194/os-18-549-2022

Cresci A. A comprehensive hypothesis on the migration of european glass eels (*Anguilla anguilla*). *Biol Rev* 2020;**95**:1273–86. https://doi.org/10.1111/brv.12609

Cushing D. Plankton production and year-class strength in fish populations: an update of the match/mismatch hypothesis. *Adv Mar Biol* 1990;**26**:249–93.

Dadswell M, Spares A, Reader J *et al.* The north Atlantic subpolar gyre and the marine migration of Atlantic salmon *Salmo salar*: The 'merry-go-round'hypothesis. *J Fish Biol* 2010;**77**:435–67. https://doi.org/10.1111/j.1095-8649.2010.02673.x

de Eyto E, McGinnity P. Fish lengths of juvenile Atlantic salmon from the Burrishoole catchment, co. mayo, ireland (1997-2019). Ireland: Marine Institute, 2023.

Diack G. Atlantic salmon smolt migration timing for 9 rivers across UK, Ireland and France. *Knowledge Network for Biocomplexity*. 2021. https://doi.org/10.5063/F1HQ3XD1 (July 2024, last accessed).

Dolmaire E. Spatial modelling of blue whiting population dynamics in the north-east Atlantic. 2022. https://doi.org/10.48730/dpx9-2d45 (October 2023, last accessed).

Døving KB, Stabell OB. Trails in open waters: sensory cues in salmon migration. In: *Sensory Processing in Aquatic Environments*. New York, NY: Springer, 2003, 39–52.

Drinkwater KF, Belgrano A, Borja A *et al.* The response of marine ecosystems to climate variability associated with the north Atlantic oscillation. *Geophys Monogr Am* 2003;**134**:211–34.

Friedland K, Manning J, Link JS *et al.* Variation in wind and piscivorous predator fields affecting the survival of Atlantic salmon, *Salmo salar*, in the gulf of maine. *Fish Manage Ecol* 2012;**19**: 22–35. https://doi.org/10.1111/j.1365-2400.2011.00814.x

Friedland KD, Hansen LP, Dunkley DA. Marine temperatures experienced by postsmolts and the survival of Atlantic salmon, *Salmo salar* l., in the north sea area. *Fish Oceanogr* 1998;**7**:22–34. https://doi.org/10.1046/j.1365-2419.1998.00047.x

Friedland KD, MacLean JC, Hansen LP *et al.* The recruitment of Atlantic salmon in Europe. *ICES J Mar Sci* 2009;**66**:289–304. https://doi.org/10.1093/icesjms/fsn210

Furey NB, Vincent SP, Hinch SG *et al.* Variability in migration routes influences early marine survival of juvenile salmon smolts. *PLoS One* 2015;**10**:e0139269. https://doi.org/10.1371/journal.pone.0139269

Gilbey J, Utne KR, Wennevik V *et al.* The early marine distribution of Atlantic salmon in the North-east Atlantic: a genetically informed stock-specific synthesis. *Fish Fish* 2021;**22**:1274–306. https://doi.org/10.1111/faf.12587

Greene CH, Pershing AJ. The response of *Calanus finmarchicus* populations to climate variability in the Northwest Atlantic: basin-scale forcing associated with the North Atlantic Oscillation. *ICES J Mar Sci* 2000;**57**:1536–44. https://doi.org/10.1006/jmsc.2000.0966

Hátún H, Chafik L. On the recent ambiguity of the North Atlantic subpolar gyre index. *J Geophys Res Oceans* 2018;**123**:5072–6. https://doi.org/10.1029/2018JC014101

Hátún H, Payne M, Beaugrand G *et al.* Large bio-geographical shifts in the north-eastern Atlantic Ocean: from the subpolar gyre, via plankton, to blue whiting and pilot whales. *Prog Oceanogr* 2009;**80**:149–62. https://doi.org/10.1016/j.pocean.2009.03.001

Hedger RD, Martin F, Hatin D *et al.* Active migration of wild Atlantic salmon *Salmo salar* smolt through a coastal embayment. *Mar Ecol Prog Ser* 2008;**355**:235–46. https://doi.org/10.3354/meps07239

Hersbach H, Bell B, Berrisford P *et al.* The ERA5 global reanalysis. *Q J Roy Meteor Soc* 2020;**146**:1999–2049. https://doi.org/10.1002/qj.3803

Holliday NP, Bersch M, Berx B *et al.* Ocean circulation causes the largest freshening event for 120 years in eastern subpolar north Atlantic. *Nat Commun* 2020;**11**:585. https://doi.org/10.1038/s41467-020-14474-y

Holm M, Holst JC, Hansen L. Spatial and temporal distribution of post-smolts of Atlantic salmon (*Salmo salar* l.) in the norwegian sea and adjacent areas. *ICES J Mar Sci* 2000;**57**:955–64. https://doi.org/10.1006/jmsc.2000.0700

Holt J, Hughes S, Hopkins J *et al.* Multi-decadal variability and trends in the temperature of the northwest European continental shelf: a model-data synthesis. *Prog Oceanogr* 2012;**106**:96–117. https://doi.org/10.1016/j.pocean.2012.08.001

Houpert L, Cunningham S, Fraser N *et al.* Observed variability of the north Atlantic current in the rockall trough from 4 years of mooring measurements. *J Geophys Res Oceans* 2020;**125**:e2020JC016403. https://doi.org/10.1029/2020JC016403

Hurrell JW. Decadal trends in the north Atlantic oscillation: regional temperatures and precipitation. *Science* 1995;**269**:676–9. https://doi.org/10.1126/science.269.5224.676

Hvidsten NA, Heggberget T, Jensen AJ. Sea water temperatures at Atlantic salmon smolt enterance. *Nord J Fresh Res* 1998;**74**:79–86.

ICES. Nasco workshop for north Atlantic Salmon at-sea mortality (WK-Salmon, outputs from 2019 meeting). *ICES Sci Rep* 2020;**69**:175.

ICES. Working group on north Atlantic Salmon (WGNAS). *ICES Sci Rep* 2023;**5**. https://doi.org/10.17895/ices.pub.22743713.v1 (September 2024, last accessed).

ICES. Working group on north Atlantic Salmon (WGNAS). *ICES Sci Rep* 2024;**6**. https://doi.org/10.17895/ices.pub.25730247.v1 (September 2024, last accessed).

Jones S, Cottier F, Inall M *et al.* Decadal variability on the northwest European continental shelf. *Prog Oceanogr* 2018;**161**:131–51. https://doi.org/10.1016/j.pocean.2018.01.012

Jonsson N, Jonsson B. Size and age of maturity of Atlantic salmon correlate with the North Atlantic Oscillation Index (NAOI). *J*

Fish Biol 2004;**64**:241–7. https://doi.org/10.1111/j.1095-8649.2004.00269.x

Kashetsky T, Avgar T, Dukas R. The cognitive ecology of animal movement: evidence from birds and mammals. *Front Ecol Evol* 2021;**9**:724887. https://doi.org/10.3389/fevo.2021.724887

Kennedy R, Rosell R, Hunter E *et al.* Programmed acoustic tags reveal novel information on late-phase marine life in Atlantic salmon, *Salmo salar*. *J Fish Biol* 2023;**102**:707–11. https://doi.org/10.1111/jfb.15292

Koul V, Tesdal J-E, Bersch M *et al.* Unraveling the choice of the north Atlantic subpolar gyre index. *Sci Rep* 2020;**10**:1005. https://doi.org/10.1038/s41598-020-57790-5

Lacroix G, McCurdy P. Migratory behaviour of post-smolt Atlantic salmon during initial stages of seaward migration. *J Fish Biol* 1996;**49**:1086–101.

Lacroix GL, McCurdy P, Knox D. Migration of Atlantic salmon postsmolts in relation to habitat use in a coastal system. *Trans Am Fish Soc* 2004;**133**:1455–71. https://doi.org/10.1577/T03-032.1

Lilly J, Honkanen HH, Rodger JR *et al.* Migration patterns and navigation cues of Atlantic salmon post-smolts migrating from 12 rivers through the coastal zones around the Irish sea. *J Fish Biol* 2023;**104**:265–83.

Lilly J, Honkanen HM, Bailey DM *et al.* Investigating the behaviour of Atlantic salmon (*Salmo salar* L.) post-smolts during their early marine migration through the clyde marine region. *J Fish Biol* 2022;**101**:1285–1300.

Liu C, Cowles GW, Churchill JH *et al.* Connectivity of the bay scallop (*Argopecten irradians*) in buzzards bay, Massachusetts, U.S.A. *Fish Oceanogr* 2015;**24**:364–82. https://doi.org/10.1111/fog.12114

Main RAK. Migration of Atlantic salmon (*Salmo salar*) smolts and post-smolts from a Scottish east coast river. MSc(R) thesis, University of Glasgow. 2021.

Malcolm I, Millar C, Millidine K. Spatio-temporal variability in the emigration times and sizes of Scottish Atlantic salmon (*Salmo salar*) smolts. *Scottish Marine and Freshwater Science* 2015;**6**. http://dx.doi.org/10.7489/1590-1 (June 2023, last accessed).

Marsh R, Haigh ID, Cunningham SA *et al.* Large-scale forcing of the European slope current and associated inflows to the north sea. *Ocean Sci* 2017;**13**:315–35. https://doi.org/10.5194/os-13-315-2017

Martin F, Hedger R, Dodson J *et al.* Behavioural transition during the estuarine migration of wild Atlantic salmon (*Salmo salar* L.) smolt. *Ecol Fresh Fish* 2009;**18**:406–17. https://doi.org/10.1111/j.1600-0633.2009.00357.x

Martín Míguez B, Novellino A, Vinci M *et al.* The European marine observation and data network (EMODnet): visions and roles of the gateway to marine data in Europe. *Front Mar Sci* 2019;**6**:313. https://doi.org/10.3389/fmars.2019.00313

Mathworks Inc. Matlab version 9.11.0.1769968 (r2023b). 2021. https://uk.mathworks.com/products/matlab.html (November 2024, last accessed).

Minkoff D, Putman NF, Atema J *et al.* Nonanadromous and anadromous Atlantic salmon differ in orientation responses to magnetic displacements. *Can J Fish Aquat Sci* 2020;**77**:1846–52. https://doi.org/10.1139/cjfas-2020-0094

Moore A, Freake S, Thomas I. Magnetic particles in the lateral line of the Atlantic salmon (*Salmo salar* L.). *Philos Trans R Soc Lond Ser B Biol Sci* 1990;**329**:11–5. https://doi.org/10.1098/rstb.1990.0145

Moriarty P, Byron C, Pershing A *et al.* Predicting migratory paths of post-smolt Atlantic salmon (*Salmo salar*). *Mar Biol* 2016;**163**:1–11. https://doi.org/10.1007/s00227-015-2782-x

Mork KA, Gilbey J, Hansen LP *et al.* Modelling the migration of post-smolt Atlantic salmon (*Salmo salar*) in the northeast Atlantic. *ICES J Mar Sci* 2012;**69**:1616–24. https://doi.org/10.1093/icesjms/fss108

Murray RO. Modelling scottish shelf seas. *Ocean Challenge* 2017;**22**:9–11

Newton M, Barry J, Lothian A *et al.* Counterintuitive active directional swimming behaviour by Atlantic salmon during seaward migration

in the coastal zone. *ICES J Mar Sci* 2021;**78**:1730–43. https://doi.or g/10.1093/icesjms/fsab024

Økland F, Thorstad E, Finstad B *et al.* Swimming speeds and orientation of wild Atlantic salmon post-smolts during the first stage of the marine migration. *Fish Manage Ecol* 2006;**13**:271–74. https://doi.org/10.1111/j.1365-2400.2006.00498.x

Otero J, L'Abée-Lund JH, Castro-Santos T *et al.* Basin-scale phenology and effects of climate variability on global timing of initial seaward migration of Atlantic salmon (*Salmo salar*). *Glob Chang Biol* 2014;**20**:61–75. https://doi.org/10.1111/gcb.12363

Ounsley JP, Gallego A, Morris DJ *et al.* Regional variation in directed swimming by Atlantic salmon smolts leaving scottish waters for their oceanic feeding grounds—a modelling study. *ICES J Mar Sci* 2020;**77**:315–25.

Pardo SA, Bolstad GH, Dempson JB *et al.* Trends in marine survival of Atlantic salmon populations in eastern Canada. *ICES J Mar Sci* 2021;**78**:2460–73. https://doi.org/10.1093/icesjms/fsab118

Peyronnet A, Friedland K, Ó Maoileidigh N. Different ocean and climate factors control the marine survival of wild and hatchery Atlantic salmon *Salmo salar* in the north-east Atlantic ocean. *J Fish Biol* 2008;**73**:945–62. https://doi.org/10.1111/j.1095-8649.2008.01984.x

Putman NF, Scanlan MM, Billman EJ *et al.* An inherited magnetic map guides ocean navigation in juvenile pacific salmon. *Curr Biol* 2014;**24**:446–50. https://doi.org/10.1016/j.cub.2014.01.017

Pyper BJ, Peterman RM. Comparison of methods to account for autocorrelation in correlation analyses of fish data. *Can J Fish Aquat Sci* 1998;**55**:2127–40. https://doi.org/10.1139/f98-104

Quinn TP. Evidence for celestial and magnetic compass orientation in lake migrating sockeye salmon fry. *J Comp Physiol* 1980;**137**:243–8. https://doi.org/10.1007/BF00657119

Renkawitz MD, Sheehan TF, Goulette GS. Swimming depth, behavior, and survival of Atlantic salmon postsmolts in Penobscot bay, maine. *Trans Am Fish Soc* 2012;**141**:1219–29. https://doi.org/10.1080/00028487.2012.688916

Rinaldo A, de Eyto E, Reed T *et al.* Global warming is projected to lead to increased freshwater growth potential and changes in pace of life in Atlantic salmon *Salmo salar*. *J Fish Biol* 2023;**104**:647–61. https://doi.org/10.1111/jfb.15603

Rodger JR, Lilly J, Honkanen HM *et al.* Inshore and offshore marine migration pathways of Atlantic salmon post-smolts from multiple rivers in Scotland, England, Northern Ireland, and Ireland. *J Fish Biol* 2024; 1–18.

Sarafanov A. On the effect of the north Atlantic oscillation on temperature and salinity of the subpolar north Atlantic intermediate and deep waters. *ICES J Mar Sci* 2009;**66**:1448–54. https://doi.org/10.1093/icesjms/fsp094

Satterthwaite WH, Carlson SM, Allen-Moran SD *et al.* Match-mismatch dynamics and the relationship between ocean-entry timing and relative ocean recoveries of central valley fall run chinook salmon. *Mar Ecol Prog Ser* 2014;**511**:237–48. https://doi.org/10.3354/meps10934

Schabetsberger R, Miller MJ, Olmo GD *et al.* Hydrographic features of anguillid spawning areas: potential signposts for migrating eels. *Mar Ecol Prog Ser* 2016;**554**:141–55. https://doi.org/10.3354/meps11824

Shelton R, Turrell W, Macdonald A *et al.* Records of post-smolt Atlantic salmon, *Salmo salar* L., in the faroe-shetland channel in june 1996. *Fish Res* 1997;**31**:159–62. https://doi.org/10.1016/S0165-7836(97)00014-3

Simpson JH, Sharples J. Introduction to the physical and biological oceanography of shelf seas. Cambridge. Cambridge University Press, 2012.

Taylor P. Experimental evidence for geomagnetic orientation in juvenile salmon, *Oncorhynchus tschawytscha* walbaum. *J Fish Bio* 1986;**28**:607–23. https://doi.org/10.1111/j.1095-8649.1986.tb05196.x

Thorstad E, Whoriskey F, Uglem I *et al.* A critical life stage of the Atlantic salmon *Salmo salar*: behaviour and survival during the smolt and initial post-smolt migration. *J Fish Biol* 2012;**81**:500–42. https://doi.org/10.1111/j.1095-8649.2012.03370.x

Thorstad EB, Rikardsen AH, Alp A *et al.* The use of electronic tags in fish research–an overview of fish telemetry methods. *Turk J Fish Aquat Sci* 2013;**13**:881–96.

Tyldesley E, Banas NS, Diack G *et al.* Patterns of declining zooplankton energy in the northeast Atlantic as an indicator for marine survival of Atlantic salmon. *ICES J Mar Sci* 2024;**81**:1164–1184. https://doi.org/10.1093/icesjms/fsae077

Utne KR, Pauli BD, Haugland M *et al.* Poor feeding opportunities and reduced condition factor for salmon post-smolts in the northeast Atlantic ocean. *ICES J Mar Sci* 2021;**78**:2844–57. https://doi.org/10.1093/icesjms/fsab163

Utne KR, Thomas K, Jacobsen JA *et al.* Salmon post-smolt, mackerel and herring stomach content. 2020. https://doi.org/10.21335/NMDC-484551947 (May 2024, last accessed).

van Deurs M, Christensen A, Rindorf A. Patchy zooplankton grazing and high energy conversion efficiency: ecological implications of sandeel behavior and strategy. *Mar Ecol Prog Ser* 2013;**487**:123–33. https://doi.org/10.3354/meps10390

Vollset KW, Lennox RJ, Lamberg A *et al.* Predicting the nationwide outmigration timing of Atlantic salmon (*Salmo salar*) smolts along 12 degrees of latitude in Norway. *Divers Distrib* 2021;**27**:1383–92. https://doi.org/10.1111/ddi.13285

Wilson SM, Buehrens TW, Fisher JL *et al.* Phenological mismatch, carryover effects, and marine survival in a wild steelhead trout *Oncorhynchus mykiss* population. *Prog Oceanogr* 2021;**193**:102533. https://doi.org/10.1016/j.pocean.2021.102533

Xu W, Miller PI, Quartly GD *et al.* Seasonality and interannual variability of the european slope current from 20 years of altimeter data compared with in situ measurements. *Remote Sens Environ* 2015;**162**:196–207. https://doi.org/10.1016/j.rse.2015.02.008

Handling Editor: Caroline Durif